ACS APPLIED NANO MATERIALS

Article

Impact of Silanization on the Structure, Dispersion Properties, and Biodegradability of Nanocellulose as a Nanocomposite Filler

Benjamin Phillip Frank, David P. Durkin, Emily Caudill, Lingchao Zhu, Donald White, Michael L Curry, Joel A. Pedersen, and D. Howard Fairbrother

ACS Appl. Nano Mater., **Just Accepted Manuscript** • DOI: 10.1021/acsanm.8b01819 • Publication Date (Web): 14 Nov 2018

ACS Publications

is published by the American Chemical Society. 1155 Sixteenth Street N.W., Washington, DC 20036

Impact of Silanization on the Structure, Dispersion Properties, and Biodegradability of Nanocellulose as a Nanocomposite Filler

Benjamin P. Frank[1], David P. Durkin[2], Emily R. Caudill[3], Lingchao Zhu[3], Donald H. White[4], Michael L. Curry[4], Joel A. Pedersen[3], D. Howard Fairbrother[1*]

[1] Department of Chemistry, Johns Hopkins University, 3400 N. Charles Street, Baltimore, MD 21218, United States

[2] Department of Chemistry, U.S. Naval Academy, 572M Holloway Road, Annapolis, MD 21402, United States

[3] Department of Chemistry, University of Wisconsin-Madison, 1101 University Avenue, Madison, WI 53706, United States

[4] Department of Materials Science and Engineering, Tuskegee University, 1200 W. Montgomery Road, Tuskegee, AL 36088, United States

* Corresponding Author: Howard Fairbrother (howardf@jhu.edu)

Keywords: Nanocellulose, silane modification, mineralization, biodegradation, dispersion, nanofibril, polymer nanocomposite

Abstract

For nanocellulose to function effectively as a nanofiller in polymers, its interfacial properties are often modified to enhance the dispersion of nanocellulose in the polymer matrix. However, the effect of different surface modification strategies on the persistence of nanocellulose in the environment is unclear. In this study, we have examined the effect of three different hydrophobic silanization reagents on the structure, dispersion properties, and biodegradability of cellulose nanofibrils (CNFs). Specifically, we modified CNFs with hydrophobic alkoxysilanes containing methyl, propyl, or aminopropyl functional groups to form silane-modified CNFs (Si-CNFs). Using a combination of analytical techniques that included ATR-IR, XPS, and solid state NMR, we demonstrated that silanization coated the CNFs with a nanometer-scale siloxane layer, the extent of which could be controlled by varying the amount of silane added to the CNFs. The stability of Si-CNFs in chloroform-based casting solutions improved compared to untreated CNFs, and scaled with extent and hydrophobicity of the siloxane coating as quantified via a mass recovery settling test. Improvements in stability in casting solutions translated into improved Si-CNF dispersion in solution-blended polyhydroxyalkanoates composites as determined with optical microscopy and SEM. Conversely, the biodegradability of Si-CNFs, assessed by tracking sample mineralization in a mixed microbial culture from an anaerobic sludge digester, was inversely related to both the degree and hydrophobicity of CNF surface modification. As mineralization of nanocellulose is rapid and facile, tracking this property served as a proportional measure of overall biodegradability. In the most extensively silanized samples, no mineralization of Si-CNFs was observed, demonstrating that a < 2 nm thick siloxane coating was sufficiently dense and uniform to prevent microbial access to the easily mineralized nanocellulose substrate. This study highlights the important and contrasting effects that changes to surface chemistry can have on the material and environmentally relevant properties of nanocellulose.

Introduction

Cellulose is a naturally abundant, biodegradable, and non-toxic covalently-linked homopolymer that consists of 2,000 to 27,000 β(1→4) linked D-glucose residues. Each glucose residue contains three hydroxyl groups which are located on the second, third, and sixth carbons. The cellulose homopolymer exists in four main allomorphs: cellulose I, II, III, and IV. Cellulose I (CI) is the native form present in plants, and of the four is the most commonly used in the fabrication of polymer composites[1]. Due to the superior mechanical and physical properties offered at the nano-scale, native cellulose is often converted to nanocellulose in the form of cellulose nanocrystals or nanofibrils (CNCs or CNFs, respectively). Both CNCs and CNFs are classified as nanomaterials due to their nano-scale widths, but they differ in their size, shape, and crystallinity.[1-2] Because of the attractive nano-derived properties of CNFs and CNCs, nanocellulose has been utilized for both traditional applications in the paper and textile industries,[3-5] as well as applications in biodegradable packaging,[6] *in vivo* medical devices,[7] and green building materials.[8] While both forms of nanocellulose are used as fillers to structurally reinforce composite materials, research often focuses on CNFs due to the improved mechanical properties afforded by their larger aspect ratio and high degree of fibril entanglement, leading to higher tensile strength and elastic modulus in polymer nanocomposites compared to CNCs.[9-10]

CNFs can be extracted from cellulosic starting material (i.e., plant matter, tunicates) via acid digestion,[11] sonication,[12-14] mechanical milling,[15] or enzyme-assisted methods.[16] The cheap and abundant precursor to CNFs (i.e., cellulose) also makes them attractive compared to other carbon-based nanofillers (e.g., carbon nanotubes (CNTs),[17] carbon fibers,[18] and glass fibers[19]). Unlike other potentially hazardous carbon-based nanofillers,[20-22] once CNFs enter the environment, they typically undergo rapid and complete mineralization[23] as a result of microbial biodegradation to yield biogas, limiting their persistence and environmental impact.[24-25] This combination of beneficial properties make CNFs attractive, environmentally friendly alternatives to synthetic nanofillers in a range of commercial applications.

Due to the limited thermal stability of nanocellulose, which can thermally decompose at temperatures as low as 120 °C, [26-27] polymer nanocomposites containing nanocellulose are often prepared through solvent casting rather than melt mixing. Solvent casting is a technique requiring the formation of a polymer-nanoparticle suspension (i.e., the casting solution), most typically in a volatile organic solvent,[28-29] although aqueous solvent casting systems do exist.[30] The stability of the nanoparticle in the casting solution is an important factor, as the nanofiller's dispersion in the polymer plays a pivotal role in determining the extent to which the desirable attributes of the filler are conferred to the nanocomposite.[31-36] However, CNFs do not disperse well in most organic solvents due to their extensive hydrogen bonding and hydrophilic nature; consequently, solvent casting well-dispersed hydrophobic polymer-CNF nanocomposite materials remains challenging. To improve CNF dispersibility in these types of polymer nanocomposites, nanocellulose has previously been chemically modified to increase its hydrophobicity through covalent functionalization with hydrophobic moieties,[37-38] the grafting of hydrophobic polymers or thiols,[39-40] and physically adsorbing hydrophobic surfactants onto its surface.[41]

While surface modification of CNF enables the production of well-dispersed polymer nanocomposites with improved material properties, the effect of these hydrophobic modifications on the persistence of nanocellulose in the environment (as measured here by its propensity to be mineralized) has received little attention. The implicit assumption appears to be that the facile mineralization of nanocellulose is not significantly impacted by these surface modifications,[39, 42-43] or is unimportant, possibly because ionic functionalizations have been shown to have little effect on its biodegradability.[44] Considering the growth projected for the nanocellulose commercial market,[45-46] an increasing quantity of modified CNFs can be expected to enter the environment during the production, transportation, use, and disposal of nanocomposite products. Consequently, the effect of common surface modification strategies on the environmental persistence of nanocellulose must be evaluated and understood.

Silanes are frequently used as modification reagents to improve the dispersion and interfacial adhesion between polymers and fillers—including nanocellulose—in composites. The improved dispersion and interfacial properties offered by silanization[37] leads to more efficient transfer of mechanical properties from nanofiller to material. Silanization and silylation[47] of cellulose and nanocellulose has been used to improve the mechanical properties of polymer composites by improving the dispersion of filler in the polymer matrix (shown with optical microscopy[48] and scanning electron microscopy[10, 49-51]), and therefore facilitating the interfacial melding between the filler and polymer.[10, 37, 52-55] For example, Kargarzadeh *et al.*, demonstrated that cellulose nanocrystals modified with *N*-(β-aminoethyl)-γ-aminopropyltrimethoxysilane displayed improved tensile strength and modulus reinforcement of unsaturated polyester resin at 2 wt% compared to unmodified nanocrystals.[53] Similarly, cellulose nanofibers modified with 3-aminopropyl triethoxysilane increased the strain to fracture resistance of poly(lactic acid) by 27% at 0.5 wt% loading, compared to a 18% decrease at the same loading of unmodified fibers.[52] The well-documented capability and utilization of silanized CNFs to improve the properties of polymeric materials motivated us to assess these materials for their biodegradability compared to unmodified CNFs. Specifically, we modified CNFs to different degrees with three common alkoxysilane reagents of varied functionality: methyl trimethoxysilane (MTMS), propyl trimethoxysilane (PTMS), and aminopropyl trimethoxysilane (APTMS). By virtue of the alkyl character of their R-groups, MTMS, PTMS, and APTMS have been shown to both increase the hydrophobicity of nanocellulose, and improve interfacial adhesion between the nanocellulose and surrounding polymer matrices as a result of improved dispersion.[37, 48]

The principal objectives of the present study were to determine (1) the effect of hydrophobic silanization on the structure of CNFs and their dispersion properties in organic solvents and polymers, and (2) the effect of the same modifications on the mineralization of nanocellulose under anoxic conditions by anaerobic bacteria as a means of assessing their biodegradability. Scanning electron microscopy (SEM), attenuated total reflectance Fourier transform infrared spectroscopy (ATR-FTIR), X-ray photoelectron spectroscopy (XPS), and solid-state ^{13}C- and ^{29}Si-nuclear magnetic resonance spectroscopy (^{13}C-NMR and ^{29}Si-NMR) were used to identify the nature of the Si-CNFs and the ability to control the extent of silanization. The effect of silane modification on CNF stability in organic solvent casting solution was quantitatively assessed by evaluating its suspended mass as a function of settling behavior in chloroform (an organic solvent commonly employed in solvent casting) after silanization. The relation between improved CNF stability in solvent-casting media and dispersion in solution-blended polymer nanocomposite materials was assessed using polyhydroxyalkanoates (PHA) composites. Finally, the effect that the extent and nature of each silane modification had on the biodegradability of nanocellulose was determined using biomethane potential tests[56] to assess the impact silane modification has on the anaerobic biotransformation of CNFs. As nanocellulose is nearly fully mineralized during anaerobic biodegradation,[23] tracking the biogas evolved from a sample is a reliable measure of its overall biodegradability.

Experimental

Materials Preparation

In this section, principal procedures are outlined, with a more detailed description of materials and methods in the supporting information (SI). Each chemical was used as received. Freeze-dried cellulose nanofibrils (CNFs) (mechanically milled) were purchased from the University of Maine Process Development Center. CNFs were modified with MTMS, PTMS, or APTMS in ethanol-water (80:20 v/v) following procedures described in the literature.[57] In brief, silane reagents were first hydrolyzed at 0.1, 1, 5, or 10 wt% (with respect to the ethanol solution) for 2 h before CNFs (0.02 g CNF mL_{EtOH}^{-1}) were added. After the solvent was removed, the silane-modified CNFs were annealed under vacuum at 110 °C (to drive condensation reactions), washed with acetone (to remove any unreacted silane reagent), and dried at 60 °C (to remove residual acetone). The final samples were then milled to a powder with a FlackTek Speed Mixer (DAC 150) using 2 mm yttrium-stabilized zirconium milling beads. In this report, it should be understood that "x wt%" of silane modification refers to the proportion of silane added to the reaction mixture (e.g. CNF modified with 5 wt% MTMS refers to the mass of silane reagent added to the functionalization mixture, not with respect to the nanocellulose). Self-condensed siloxane polymers were also prepared in the absence of CNF under the same conditions used for CNF modification. All samples were milled to a similar consistency before evaluating their mineralization or dispersion characteristics.

Throughout this manuscript, Si-CNFs are referred to first by a number that reflects the amount of silane (wt% with respect to the reaction solution) used during CNF modification, followed by: 'Me', 'P', or 'A' referring to methyl-(Me), propyl-(P), and aminopropyl-(A) trimethoxysilane, respectively. For example, '5Me-CNF' refers to CNFs treated with a reaction solution containing 5 wt% methyl trimethoxysilane. Similarly, self-condensed siloxane polymers are labeled 'Me-self', 'P-self', and 'A-self' for methyl-, propyl-, and aminopropyl- trimethoxysilane self-condensed polymers, respectively.

Materials Characterization

Succinct descriptions of techniques used in the characterization of samples are provided below, while full details of characterization methods are found in the SI. In brief, the morphology of CNFs before and after silane modification was analyzed using scanning electron microscopy (SEM); the functional groups in the unmodified CNF and in each of the Si-CNFs were identified using attenuated total reflectance Fourier transform infrared spectroscopy (ATR-FTIR); the bonding and concentrations of C, O, N, and Si at the surface of the unmodified CNF and Si-CNFs was assessed using X-ray photoelectron spectroscopy (XPS); the carbon structure of the nanocellulose before and after modification and the form of the silane reagents after CNF modification and self-condensation were identified via solid-state ^{13}C- and ^{29}Si- nuclear magnetic resonance spectroscopy (NMR); the amount of Si in the Si-CNFs was quantified with energy dispersive X-ray spectroscopy (EDS); and the dispersion of CNFs in solvent-cast polymer nanocomposites was assessed using optical microscopy (OM), SEM, and EDS.

Supernatant Mass Recovery Tests

The effect that silane modification had on CNF stability in an organic solvent casting solution was investigated via mass recovery analysis performed on the supernatant of chloroform solutions containing unmodified and silane-modified CNFs. In these experiments, CNFs were sonicated in chloroform for 5 h to form a suspension at a concentration representative of those used in solvent casting syntheses[58] (0.5 mg $CNF \cdot mL_{solvent}^{-1}$). At select time-points (settling times) after the suspension had been formed, 10 mL aliquots of supernatant were removed from the suspension, collected, dried on a 60 °C hotplate, and then weighed to determine the CNF concentration in the supernatant. Triplicate samples of the unmodified CNFs were run to determine the precision of this method. The baseline for detectable suspended concentration was determined through a blank control sample of chloroform run without any nanocellulose, prepared identically to the CNF samples and tracked over 100 h. Results from this study revealed that the baseline level for CNF detection is roughly 7% of the initial CNF concentration. The nonzero concentration value detected is due to contaminant species from sonication (i.e., silica) being present in suspension at low concentrations (< 1 $mg \cdot 10\ mL_{EtOH}^{-1}$).

Synthesis of Hydrophobic Solvent Cast Polymer Nanocomposites

To relate changes in the stability of CNFs in chloroform after silanization to their dispersion in a hydrophobic material, polymer nanocomposites were synthesized via a solution casting process where chloroform was used as the solvent. CNFs were suspended in chloroform via sonication at the same concentration used in the dispersion studies (equivalent to 5 wt% in polymer) before polyhydroxyalkanoates (PHA) were added at a concentration of 10 $mg \cdot mL_{solvent}^{-1}$, and sonicated for an additional 2 h. The PHA used in these experiments was a co-polymer of poly-3-hydroxybutyrate (P3HB) and poly-4-hydroxybutyrate (P4HB), purchased from Yield10Bioscience (formerly Metabolix Inc., Woburn, MA) Aliquots of this casting solution (5 mL) were poured in ~40 mm diameter aluminum dishes and dried to evaporate the chloroform, leaving behind a solvent-cast thin film composite of 5 wt% CNF in PHA. This procedure was performed with both unmodified CNFs and 5Me-CNFs, the latter used as a representative Si-CNF. CNF dispersion in both composites was determined using OM and SEM images of the nanocomposite surfaces.

Biogas Production Tests

The mineralization of unmodified CNFs and Si-CNFs was assessed using biomethane potential (BMP) tests to track biogas production when the samples were exposed to an anaerobic mixed microbial culture. In brief, a bacterial media was prepared using nutrient and buffers as outlined in Angelidaki, *et al.*[59] The media was heated at 100 °C for 30 min to achieve anoxic conditions before it was inoculated with a culture sourced from anaerobic digester sludge (obtained from Back River Waste Water Treatment Plant, Baltimore, MD) at a concentration of 10% v/v. The BMP media was then adjusted to a pH of 7.2 and kept anoxic via continuous purging with N_2 gas throughout the preparation. CNF samples were combined with the N_2-purged anaerobic bacterial media in septum-sealed bottles (in triplicate) and reacted at mesophilic temperature (35 °C). As CNFs and Si-CNFs underwent mineralization, the evolution of biogas produced a positive pressure within the sealed system which was tracked via volume measurements using a glass syringe. In this way, the volume of biogas measured provided a direct quantification of the pressure increase within the bottles stemming from the evolved biogas. Triplicate samples of blank anaerobic media were also prepared to determine the biogas produced from residual native organic matter in the sludge. Values from these blanks (typically < 3 mL per time point) were subtracted from each nanocellulose sample to determine the volume of biogas produced due to each CNF alone. Gas composition was also assessed. The rate, magnitude, and change in composition of biogas evolution were determined by measuring the biogas produced at various time points ranging from 3 to 120 days.

Exact sample mass added to each bottle was adjusted to ensure the same amount of biodegradable material (i.e., ~150 mg of nanocellulose) was available in each sample regardless of the silanization. This was accomplished by estimating the overall degree of silanization in each sample based on the atomic % Si determined by EDS (Table S1). For example, based on EDS data, 0.1Me-CNF contained approximately one equivalent of silicon-containing reagent for each cellobiose unit (disaccharide composed of two β-glucose residues linked by a β(1→4) bond). As a result, roughly 163 mg of 0.1Me-CNF was added to each bottle based on the assumption that each silicon atom represented the addition of one ($MeSiO_3$) unit to the cellulose structure. In addition to controlling the mass of each sample that went into the bioreactors, the volume of CH_4/CO_2 produced by each sample was benchmarked to the maximum biogas produced by an unmodified CNF control exposed to the same bacterial culture.

Results

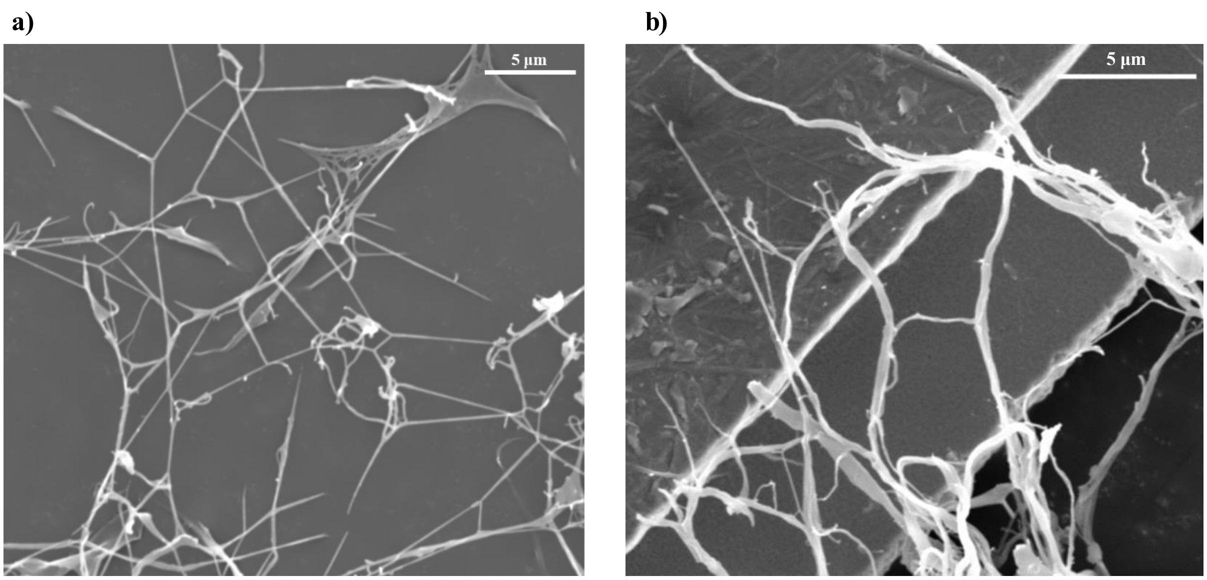

Figure 1. Scanning electron microscopy (SEM) images of (a) unmodified cellulose nanofibrils (CNF) and (b) CNFs modified with 10 wt% propyl trimethoxysilane (10P-CNF). SEM images were taken at 10 kV.

Characterization of CNFs and Si-CNFs

CNF samples were modified with one of three trialkoxysilane reagents (MTMS, PTMS, or APTMS). The amount of silane used in each modification reaction was varied (i.e., 0.1 – 10 wt%) to obtain three series of silane-modified CNFs for characterization. In addition, each silane reagent was self-condensed in the absence of CNF to form siloxane polymers (Me-self, P-self, A-self) for comparison. Samples were analyzed with a combination of SEM, ATR-FTIR, solid-state ^{13}C- and ^{29}Si-NMR, and XPS/EDS to determine the nature of the silane modification.

The morphology of the unmodified and silane-modified CNFs was characterized with SEM (representative images in Figure 1). The identification of cellulose nanofibrils was confirmed via the nanometer-scale widths (101 +/- 17 nm) and micron-scale lengths that were observed.[60] The persistence of these characteristic aspect ratios after silanization indicates that the nanocellulose maintained its nanofibril structure after silane treatment.

Infrared spectra of the 5Me-CNF, 5P-CNF, 5A-CNF, and unmodified CNF powders are presented in Figure 2a. For unmodified CNF, the principal peaks for cellulose were observed (i.e., C–O stretching at 1035 cm^{-1}, C–H stretching region at 2900 cm^{-1}, and broad O-H stretching centered at 3350 cm^{-1}).[61] In addition to the characteristic cellulosic peaks, Si-CNFs also displayed new IR peaks which are unique to each respective silane reagent; specifically, Si–CH_3 symmetrical deformation at 766 cm^{-1} and 1270 cm^{-1} for MTMS-modified CNF;[62-63] methylene stretching peaks at 2880 cm^{-1} and 2950 cm^{-1} for PTMS-modified

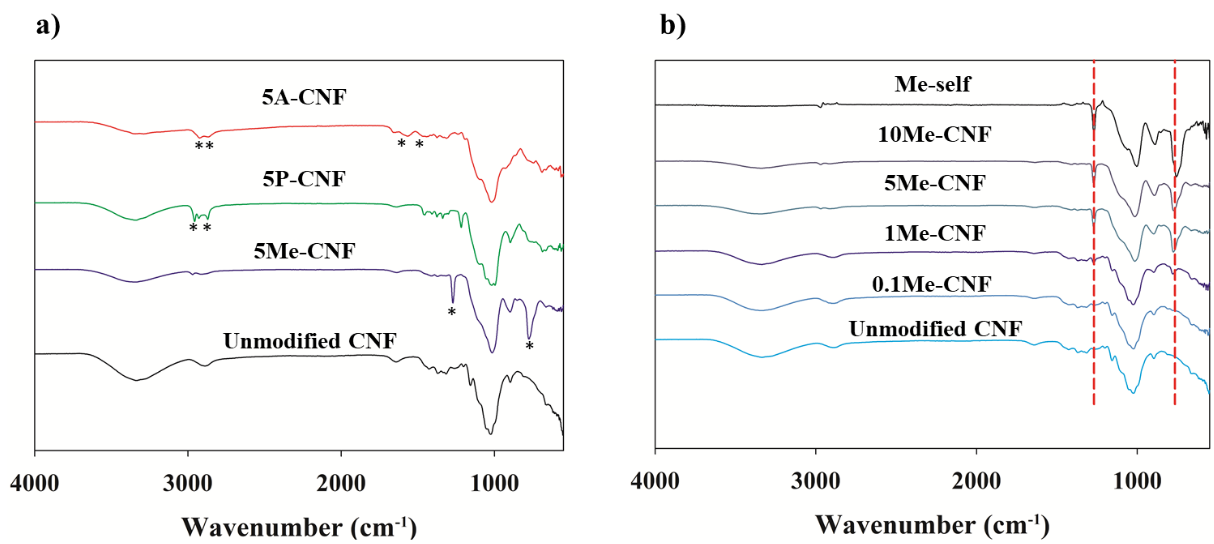

Figure 2. Attenuated total reflectance Fourier transform infrared spectroscopy (ATR-FTIR) of (a) cellulose nanofibrils (CNFs) modified with 5 wt% methyl(Me)-, propyl(P)-, or aminopropyl(A)-trimethoxysilane, and (b) CNFs modified with increasing amount of methyl trimethoxysilane (0 through 10 wt%) compared to the methyl trimethoxysilane self-condensate (Me-self). Relevant silane peaks in Figure 2a are marked with an *. Silane peaks in Figure 2b annotated with red dotted line. All spectra were normalized to the cellulose peak at 1035 cm^{-1} to facilitate direct comparison.

CNF;[64-65] and methylene stretching modes at 2920 cm^{-1} and 2860 cm^{-1}, as well as N–H scissoring at 1580 cm^{-1} and symmetric deformation of NH_3^+ at 1480 cm^{-1} for APTMS-modified CNF.[66-67] The ATR-FTIR data also revealed that the intensity of each silane peak increases systematically with the degree of silanization. For example, ATR-FTIR data of MTMS-modified CNF in Figure 2b show a clear increase of the peaks at 766 cm^{-1} and 1270 cm^{-1} with an increasing degree of silane modification.

XPS was used to characterize the elemental composition and bonding environment of atoms in the near surface region (≲ 2-3 nm) of the unmodified and Si-CNFs (Figures 3 and S1). Figure 3a shows the high-resolution C(1s), O(1s), and Si(2p) photoelectron peaks obtained from CNFs modified with MTMS. The C(1s) envelope of the unmodified CNF is comprised of three components and is consistent with previous measurements of nanocellulose.[68] The envelope consisted of a dominant peak at 286.6 eV due to the presence of C–O bonding, a higher binding energy O–C–O peak at 288.3 eV due to the acetal linkage in nanocellulose, and a peak at 284.8 eV likely due to adventitious carbon. Figure 3a shows that the intensity of the photoelectron transition at 284.8 eV (due to C–C or C-Si bonding)[68] in MTMS-modified CNF increased systematically with silane loading due to the introduction of Si–C carbon atoms. In contrast, the

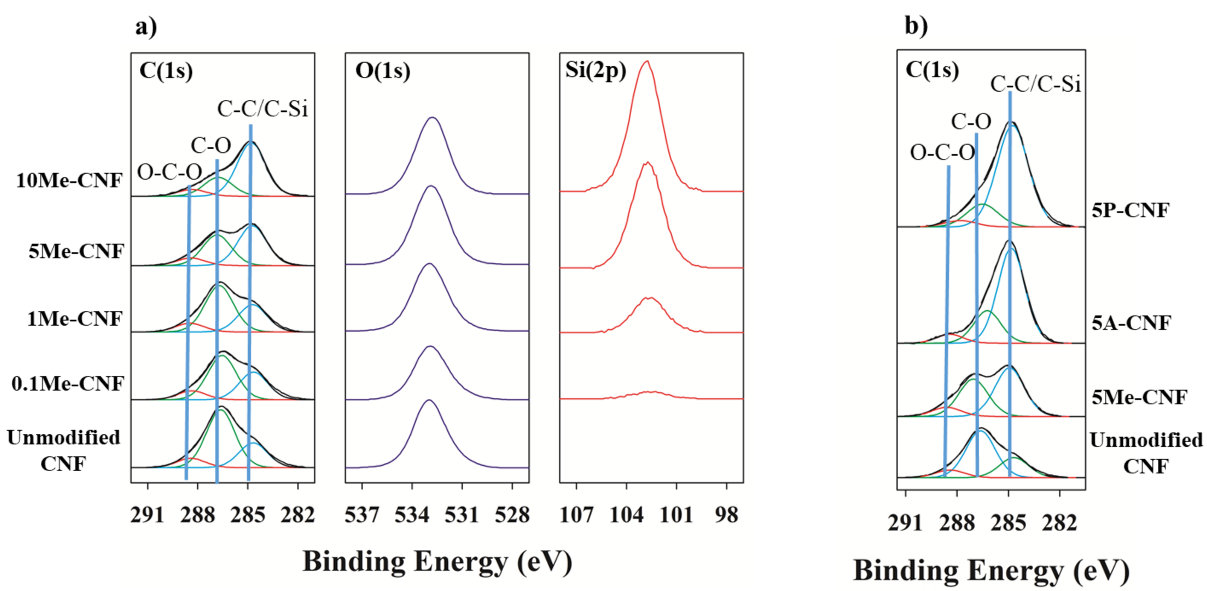

Figure 3. X-ray photoelectron spectroscopy (XPS) of (a) C(1s), O(1s), and Si(2p) regions for cellulose nanofibrils (CNFs) modified with different wt% methyl trimethoxysilane, and (b) C(1s) region for CNFs modified with 5 wt% methyl(Me)-, propyl(P)-, or aminopropyl(A)- trimethoxysilane.

C–O and O–C–O peaks decreased in intensity as silanization increased. Additionally, as the degree of silanization increased, the concentration of Si generally increased in both XPS (Figure 3a) and EDS (Table S1). Figure 3b compares the C(1s) regions for unmodified CNFs as well as 5Me-, 5P-, and 5A-CNF. Although the C(1s) envelopes contain the same three peaks, the C–C/C–Si peak intensity in 5A-CNF and 5P-CNF is larger than in 5Me-CNF due to the greater number of carbon atoms in the side chain of APTMS and PTMS reagents compared to MTMS. Consistent with expectations, nitrogen was observed only in the APTMS-modified CNFs (data not shown), and steadily increased in concentration as the amount of APTMS used in modifying the CNFs increased.

To further characterize the nature of the CNFs before and after silanization, solid-state ^{29}Si- and ^{13}C-NMR were performed on the unmodified, 5Me-, 5P-, and 5A-CNFs as well as the self-condensed polymers (Me-self, P-self, and A-self). The ^{13}C-NMR spectrum of untreated nanocellulose with peak assignments is shown in Figure 4a along with the spectra of the three self-condensed and three Si-CNF samples. The peaks between 50 and 150 ppm in the CNF-containing spectra reflect carbons C-1 through C-6 (labeled in Figure S2) of cellulose in both amorphous and crystalline forms. Peaks corresponding to crystalline and amorphous forms of cellulose in the unmodified CNF spectrum were assigned based on known chemical shifts.[69] In this cellulosic region, the spectra of unmodified CNFs and Si-CNFs were similar, as evinced by the peak shifts in Table S2. The peaks between 0 and 50 ppm in the ^{13}C-NMR spectrum arose from the R_1 alkyl side chains (methyl, propyl, and aminopropyl) from the silanization reagents, and are comparable between the self-condensed and Si-CNF spectra. The methylene carbons in the aminopropyl side chain produced peak shifts at 11.7, 24.6 and 43.6 ppm; this reflected the different chemical environments of the three side chain carbons. The methylene and methyl carbons of the propyl side chain produced peak shifts at 15.9 and 16.9 ppm, with a visible shoulder around 17.8 ppm. The methyl

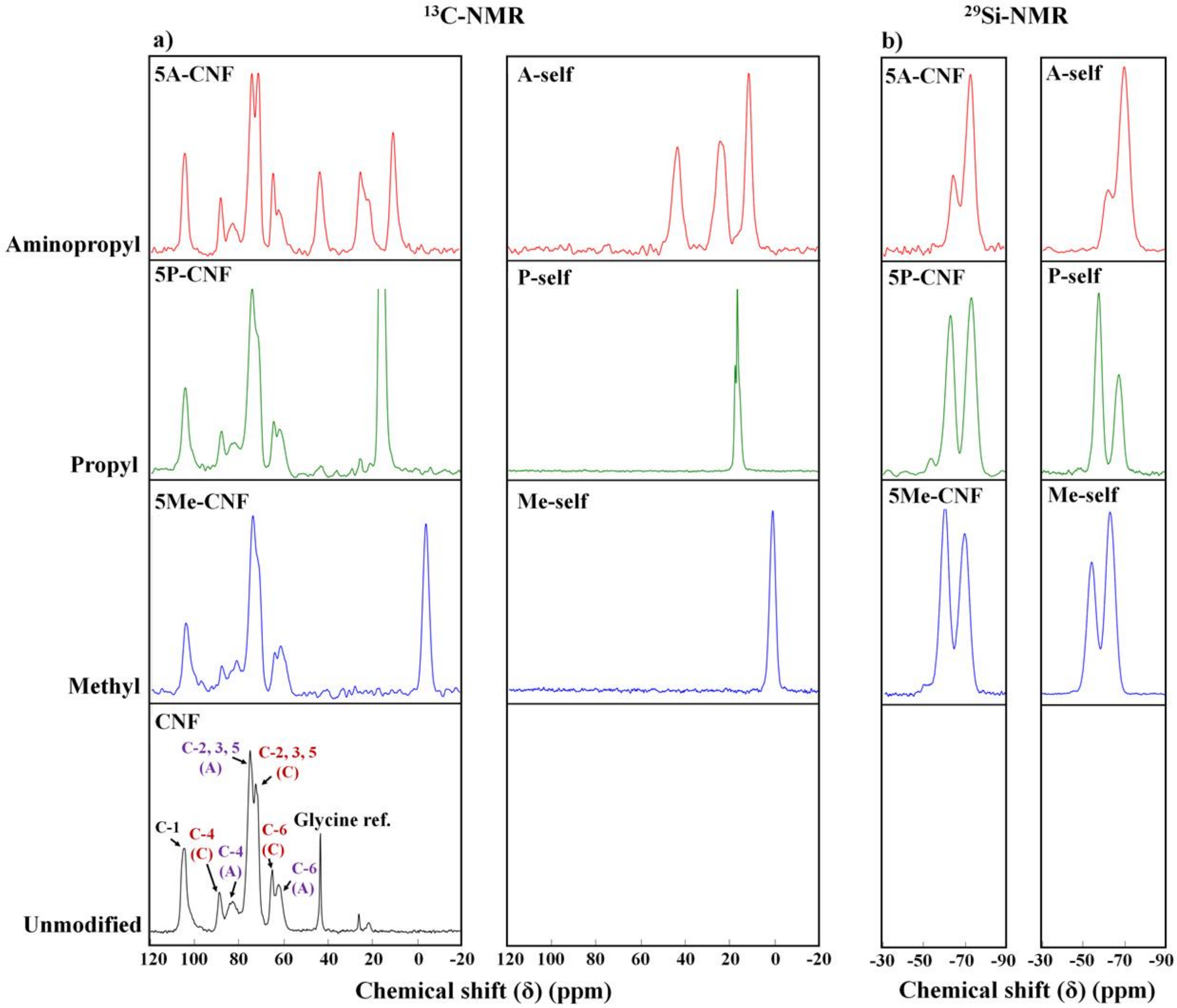

Figure 4. Solid-state ^{13}C-NMR spectra (a) of cellulose nanofibrils (CNF) modified with 5 wt% aminopropyl (5A-CNF), propyl (5P-CNF), or methyl (5Me-CNF) trimethoxysilane (Si-CNFs) compared to self-condensed silane reagents (A-self, P-self, Me-self). In unmodified CNF, characteristic peaks are designated by amorphous ('A', purple), crystalline ('C', dark red), or peaks where the amorphous and crystalline regions are convoluted (black) labels. Shown on the right is solid state ^{29}Si-NMR spectra (b) of Si-CNFs modified with 5 wt% aminopropyl (5A-CNF), propyl (5P-CNF), or methyl (5Me-CNF) trimethoxysilane compared to self-condensed silane reagents (A-self, P-self, Me-self).

side chain produced a large, single peak between 0 and 1 ppm. The ^{29}Si-NMR spectra of both the self-condensates and Si-CNFs is shown in Figure 4b with relevant chemical shifts in Table S3. The T^i notation used herein indicates that each silicon atom in the silane coupling agents can have three (T) Si–O–R bonds and one bond to a sidechain group (Si–R_1; the R_1 sidechains are methyl, propyl, or aminopropyl in these experiments). The i denotes the number of Si–O–R bonds that bridge to another silicon atom (Si–O–Si).[70]

The remaining Si–O–R bonds bridge to either H, CH_3, or cellulose in these experiments. Hence, in addition to the R_1 sidechain, a T^1 silicon atom has one siloxane (Si–O–Si) bridge and two Si–O–R bridges; a T^2 silicon atom has two Si–O–Si bridges and one S–O–R bridge; and a T^3 silicon atom has three Si–O–Si bridges and zero Si–O–R bridges. The T^1 silicon atoms produce ^{29}Si peak shifts between –44 and –49 ppm; T^2 silicon atoms result in peaks around –53 to –57 ppm; and T^3 silicon atoms present peak shifts near –68 ppm.[70-73]

In the Si-CNFs and the self-condensed siloxane polymers (i.e., with no CNF present), the ^{29}Si-NMR showed no chemical shifts near –40 ppm, where T^0 and nonhydrolyzed silicon atoms would be detected.[70, 72, 74] This indicates that the methoxy groups of the trimethoxysilane reagents underwent complete hydrolysis and subsequent self-condensation to produce peak shifts reflecting T^1, T^2, and T^3 silicon atoms.

The ^{29}Si-NMR spectra of the self-condensed and Si-CNF samples are comparable as each are dominated by the presence of T^2 and T^3 silane species (Figure 4b). For the self-condensed materials, the more downfield peaks are centered between about –53 and –62 ppm (T^2 forms), and the peaks upfield of this are between approximately –62 and –68 ppm (T^3 forms), with variations in position reflecting the influence of the electron donating character of the R_1 side chains (methyl, propyl, aminopropyl).[75-77] This effect is exhibited by both the self-condensates and the Si-CNFs: the chemical shifts for each type of silicon atom (i.e., T^i designation) are lowest for the aminopropyl trimethoxysilane reagent, followed by the propyl and then the methyl trimethoxysilanes (Table S3). For the Si-CNF materials, the T^2 peaks are between about –59 and –63 ppm, and the T^3 peaks are between approximately –68 and –72 ppm.

A much smaller, but detectable T^1 silicon peak was present (between –44 to –48 ppm) in the spectra of the self-condensates of only the propyl and methyl trimethoxysilanes, and not in those of the aminopropyl self-condensate sample. A smaller T^1 peak was apparent in all Si-CNF spectra, estimated between –44 and –53 ppm. The general observation of T^2 and T^3 peaks dominating the spectra with little T^1 signal is consistent with previous reports for silane-treated cellulose.[72, 78] In summary, the ^{29}Si-NMR spectra are comparable between the self-condensates and silane-treated cellulose samples, although, as expected, the chemical shifts and peak ratios varied.

Stability of Si-CNFs in Solvent Casting Media

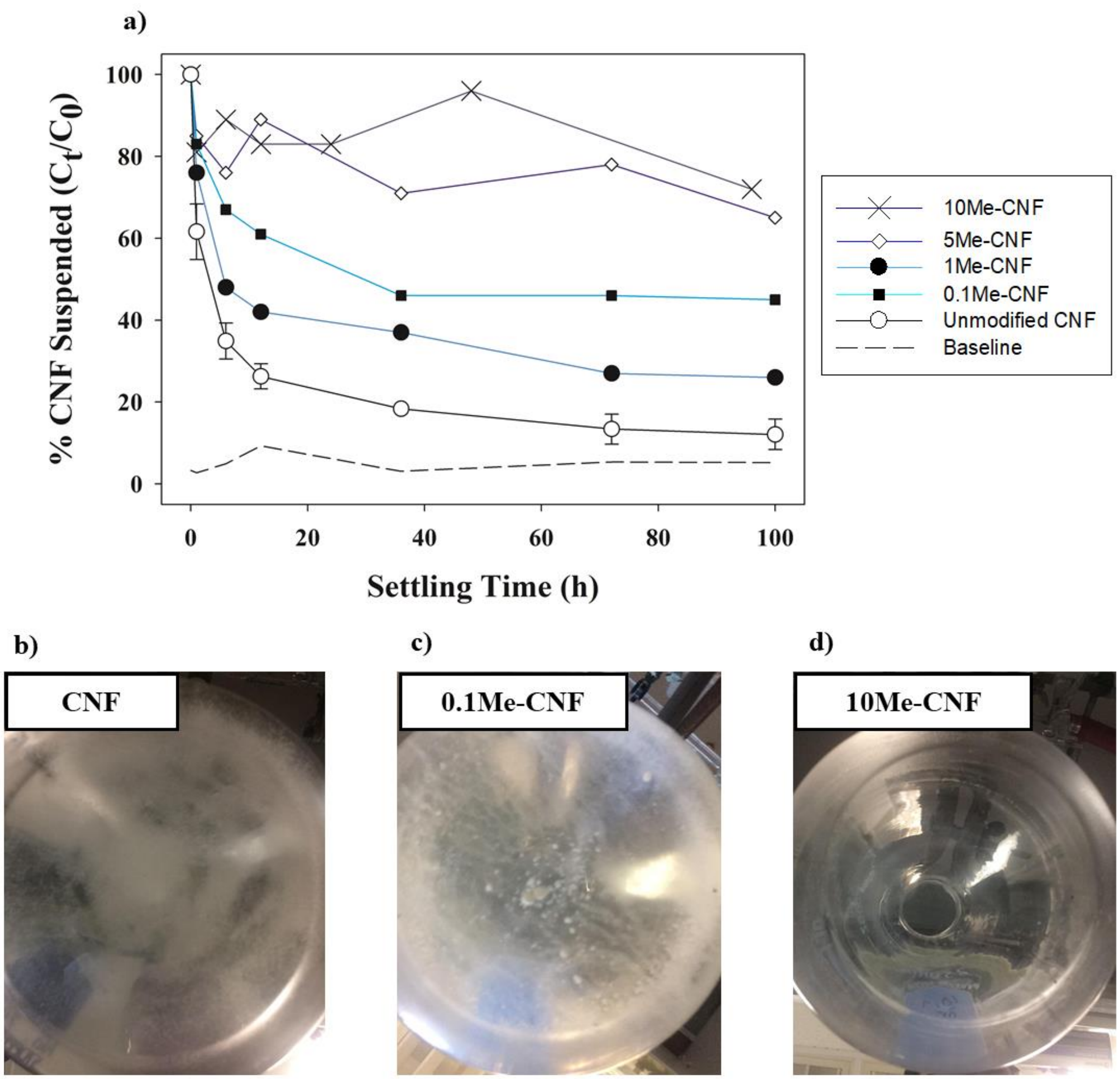

Figure 5. Stability of cellulose nanofibrils (CNFs) in chloroform, including (a) mass recovery analysis for CNFs modified with 0.1 (black squares), 1 (black circles), 5 (white diamonds), or 10 (crosses) wt% methyl trimethoxysilane compared to unmodified CNFs (white circles). Data are plotted in terms of percent CNF concentration remaining in the supernatant (C_t/C_0) as a function of settling time. The baseline concentration that could be determined via control studies is denoted by the dashed line (see text for details). Also shown are digital images of chloroform solutions containing (b) unmodified CNF, (c) 0.1Me-CNF, and (d) 10Me-CNF after 100 h settling.

Mass recovery analysis was used as a quantitative means to assess the stability of chloroform suspensions made with unmodified CNFs and Si-CNFs. This technique involved dispersing each type of CNF in chloroform and measuring the CNF/Si-CNF concentration remaining in suspension as a function of settling time. Results of mass recovery analyses for CNFs before and after silanization are presented in Figure 5 and Figure S3.

In each test, the largest decrease in CNF concentration occurred within the first 12 h of settling, followed by a relatively stable suspended concentration for the remaining 88 h. Most of the unmodified CNFs (~70%) sedimented out of suspension during the initial 12 h, which approached the baseline level of detection (Figure 5a). As the extent of silanization increased, CNF stability in chloroform generally increased. All of the Si-CNFs were present at a higher concentration in the supernatant after 100 h of settling compared to unmodified CNF. 5Me-CNF and 10Me-CNF were the most stable in chloroform; ~80% of the initial 10Me-CNF concentration remained in suspension after 100 h. In contrast, < 20% of the unmodified CNFs remained in suspension during the same time period. In the unmodified CNF and 0.1Me-CNF (Figure 5b and 5c), a significant quantity of nanocellulose was observed at the bottom of the flask. The improved stability of 10Me-CNF, in contrast, is demonstrated visually in photographs of representative CNF suspensions after 100 h of settling (shown in Figure 5d) via the lack of settled material. The 10Me-CNF solution featured a suspended layer of gel which appeared translucent with no visible particles at the bottom. The presence of 10Me-CNF siloxane in this gel layer was confirmed after 100 h of settling using transmission infrared spectroscopy (data not shown). Furthermore, the hydrophobicity of the silanization strategy (Me, P, or A) appeared to impact CNF stability. Thus, while 5A-CNF displayed improved stability compared to unmodified CNF, it was less stable than CNFs treated with the more hydrophobic reagents (5Me-CNF or 5P-CNF) as shown in Figure S3.

Dispersion of Si-CNFs in Polyhydroxyalkanoates (PHA)

Polymer nanocomposites were prepared through a solution blending of polyhydroxyalkanoates (PHA)—a hydrophobic polymer—and CNFs in chloroform followed by solvent casting thin films. Figure 6 shows images of representative films containing unmodified CNF and 5Me-CNF nanofillers. Nanocomposites made with unmodified CNF showed extensive aggregation, visible as areas of white

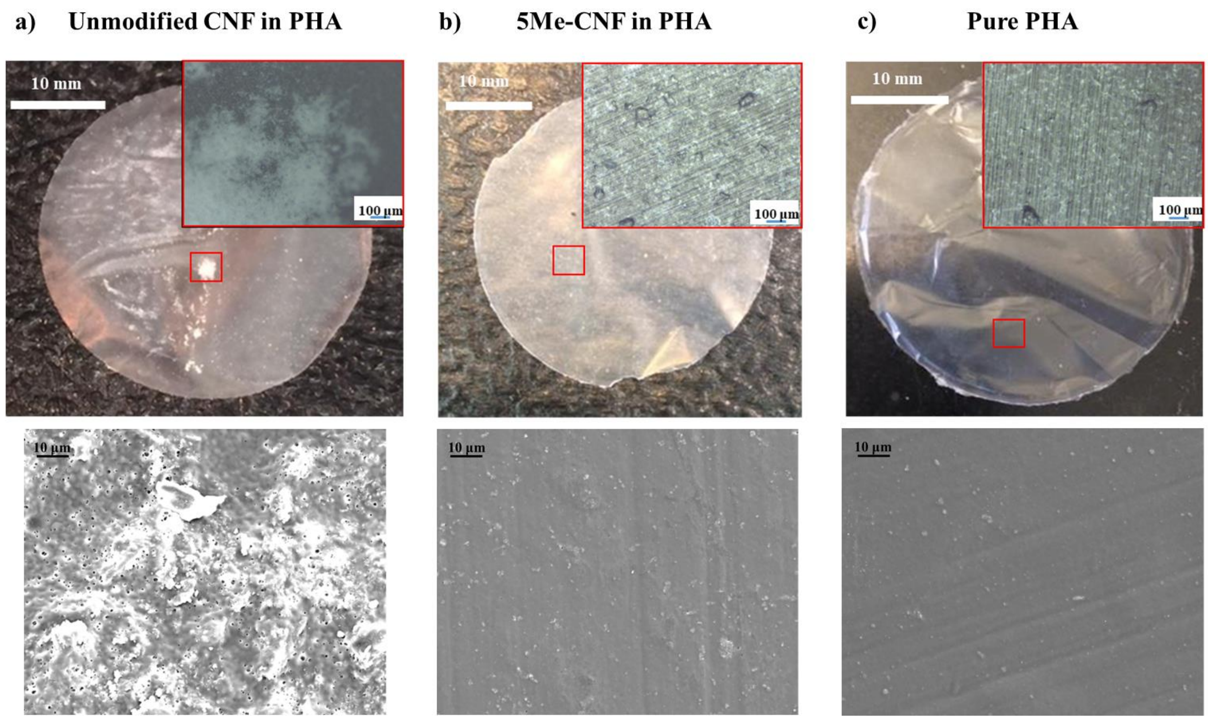

Figure 6. (Top) Digital and optical microscopy (OM, inset) images of polyhydroxyalkanoates (PHA) nanocomposites containing (a) unmodified cellulose nanofibrils (CNF), (b) CNFs modified with 5 wt% methyl trimethoxysilane (5Me-CNF), and (c) pure PHA. In each digital image, a red box highlights the region scanned with OM shown in the 1 mm^2 inset images. (Bottom) Comparative SEM images of the nanocomposite surface (10 kV, 1000x) corresponding to each sample.

patches throughout the film in Figure 6a. Optical microscopy of these areas (Figure 6a, top inset) confirmed that these aggregates were not seen in virgin PHA films (Figure 6c). Upon closer inspection with the optical microscope, these aggregates appeared to be white, fluffy particles indicative of poorly dispersed CNF. In contrast, PHA films prepared with 5Me-CNF (Figure 6b) displayed no visible white aggregates. These differences are even more apparent in the corresponding SEM images (Fig 6 bottom and Fig S4). The SEM images of PHA and PHA filled with Si-CNF were flat and largely featureless. In contrast, the PHA loaded with native CNF exhibited a rough surface with many micron sized pores. Closer investigation of the brighter features on the surface revealed the presence of fibril-like features which were distinct and detached (Fig S5) from the surrounding polymer matrix. EDS mapping (example shown in Fig S6) consistently showed that these structures possessed a higher concentration of oxygen than the surrounding PHA ($C_4O_2H_6$), as would be expected by an oxygen-rich nanocellulose fibril ($C_6O_5H_{10}$). In summary, the OM and SEM images both support the idea that Si-CNFs disperse far more uniformly in hydrophobic PHA polymer than unmodified CNFs. Moreover, in the absence of silanization, the addition of CNFs severely impacts the structural integrity of the hydrophobic polymer matrix.

Biodegradability of Si-CNFs Assessed via Mineralization

While unmodified CNFs completely and rapidly mineralize, the properties of fibrils treated with hydrophobic surface modifiers could differ.[79] Biomethane potential (BMP) tests measure the rate and extent of biogas production as a result of sample mineralization during anaerobic biodegradation, and therefore provide a quantitative method to evaluate how different silane modifications impact the extent and ease of CNF mineralization.[59] The results of BMP tests performed on unmodified and silane-modified CNFs are presented in Figure 7 and 8. All plots were normalized to the maximum volume produced by the unmodified CNF sample in each set, to account for any differences in bacterial culture obtained from separate visits to the waste water treatment plant. The biogas produced from each Si-CNF relative to unmodified CNFs as a function of inoculation time is shown in Figure 7. The biogas production curves typically displayed a sinusoidal shape. These curves provided information on both the rate and extent of each sample's mineralization, the latter expressed by the plateau point in biogas production. For CNFs modified with the lowest amount of silane reagent (i.e., 0.1Me-, 0.1P-, 0.1A-CNF), the extent of mineralization was similar

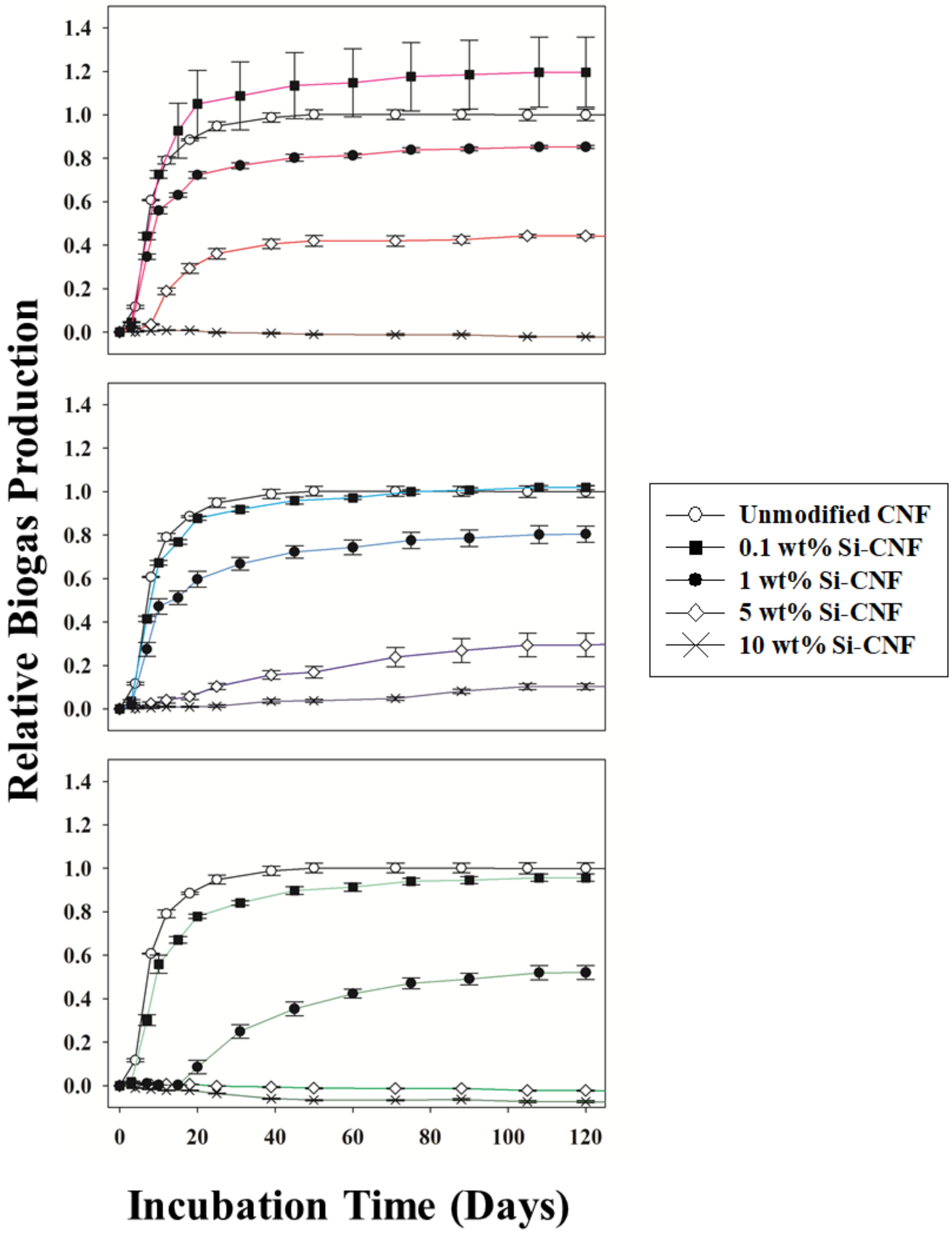

Figure 7. Relative biogas production for unmodified cellulose nanofibrils (white circles, CNFs) and CNFs modified with aminopropyl- (top), methyl- (middle), or propyl- (bottom) trimethoxysilane. Each plot displays CNFs modified with 0.1 (black squares), 1 (black circles), 5 (white diamonds), or 10 (crosses) wt% of the respective silane. Values are normalized to the biogas produced from the unmodified CNF sample under the same experimental conditions.

to that for the unmodified CNF, and each Si-CNF completely mineralized within ~20 d. However, as the extent of silane modification increased beyond this point, the inhibition of biogas production began. This effect was first observed in 1Me-, 1P-, and 1A-CNF as the total volume of biogas produced decreased as compared to the unmodified CNF. For 5Me-CNF, 5P-CNF, and 5A-CNF, a delay in the onset of biogas production was observed along with a further decrease in the total amount of biogas produced. Specifically, 29%, 0%, and 42% of the biogas produced by the unmodified CNF sample was observed for 5Me-CNF, 5P-CNF, and 5A-CNF, respectively. The suppression of biogas production was still more apparent for 10Me-, 10P-, and 10A-CNF, where there was essentially no biogas produced. Separate control studies performed to assess the mineralization of the self-condensed siloxane polymers (Figure S7) each yielded no biogas over 80 days of inoculation. Gas chromatography analysis of biogas produced across all samples showed a decrease in N_2 content (used to backfill anaerobic samples at the start of test) as biodegradation proceeded, while the carbon dioxide and methane components grew in intensity (data not shown). This trend was exhibited by all CNF samples as they were mineralized, regardless of the specific silanization. Additionally, the extent and rate of CNF mineralization were impacted by the nature of the silane reagent as shown in Figure 8, although this effect was less pronounced than the influence of the extent of

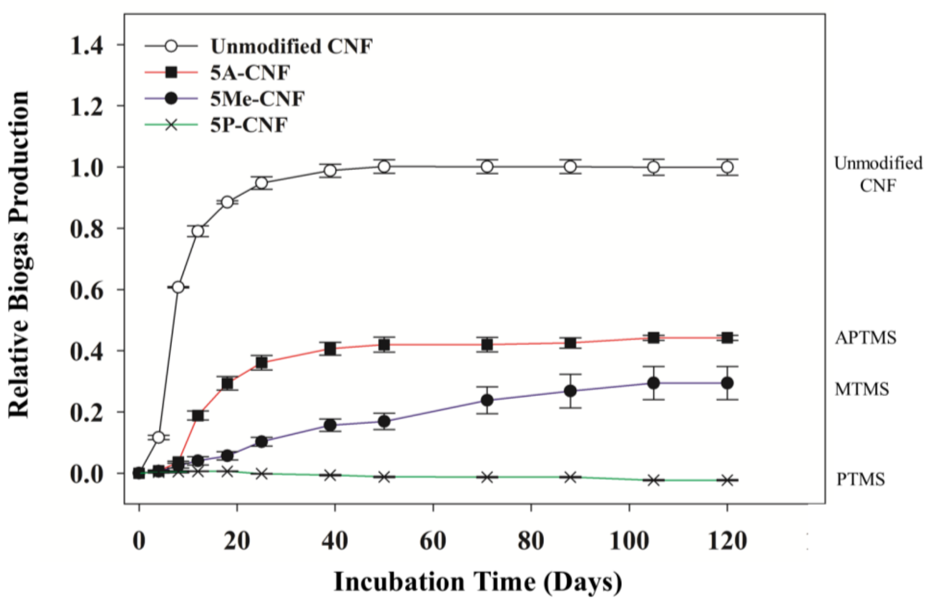

Figure 8. Relative biogas production for unmodified cellulose nanofibrils (CNF, white circles) and CNFs modified with 5 wt% aminopropyl- (squares), methyl- (black circles), or propyl- (crosses) trimethoxysilane. Values are normalized to the biogas produced by an unmodified CNF sample under

silanization. Specifically, for the same amount of added silane (here 5 wt%), the extent and rate of CNF mineralization followed the trend: unmodified CNF > 5A-CNF > 5Me-CNF > 5P-CNF.

Discussion

Characterization of Si-CNFs

After extensive silane modification, representative SEM images (Figure 1b) coupled with ATR and ^{13}C-NMR spectra (Figure 2a and 4a, respectively) of 5Me-CNF revealed that the nano-scale fibril structure and bonding of the CNFs was maintained. The ^{13}C-NMR spectra of the unmodified CNFs and the Si-CNFs (Figure 4a) additionally demonstrated that the nanocellulose samples contained characteristic peaks of both amorphous and crystalline cellulosic regions before and after treatment with the silane coupling reagents (Table S4). Based on averages of all the carbons shown in Table S4, it was concluded that the amorphous character of the CNFs was only slightly changed after silanization for each Si-CNF. This is important to establish, as differences in crystallinity are known to affect relative biodegradability between samples[80-81].

Infrared and XPS data demonstrate our ability to control the degree of silanization by tuning the amount of silane added to the reaction mixture. Thus, vibrational features associated with the silane in the ATR-FTIR spectra of MTMS-modified CNFs grew in intensity as more silane was added to the reaction mixture (Figure 2b). Additionally, increasing the degree of silanization led to an increase in the Si signal and C–C/C–Si peak intensity measured by XPS (Figure 3a), and the Si signal measured by EDS (Table S1).

The ATR-FTIR spectra of the Si-CNFs contained peaks associated with both the unmodified CNF and the respective self-condensed siloxane polymer (Figures 2a and S8). This suggested that the chemical bonding in the silane layer was similar to that of the self-condensed polymer. The solid-state ^{29}Si-NMR experiments supported this interpretation of the ATR-FTIR data, and provided insight into whether the silanes may be solely covalently bound to cellulose, or exist as self-condensed polymers. Specifically, the ^{29}Si-NMR spectra of all Si-CNFs (Figure 4b) indicated that considerable self-condensation of the silane reagents occurred as evidenced by the preponderance of T^2 and T^3 silicon atoms in the samples.

T^3 silanes are unavailable to undergo reaction with nanocellulose while T^1 or T^2 silicon atoms in the Si-CNFs may covalently bond to the nanocellulose through the formation of Si–O–cellulose bonds. Within the T^1 or T^2 peak shifts for the Si-CNFs, we could not directly discern whether the Si-O-R bonds were a Si–O–H bridge or a Si–O–cellulose bond formed after reaction with an O–H group in the CNFs. However, some degree of covalent bonding between the silane and CNF is likely as the T^1 peaks of the propyl and methyl trimethoxysilane-treated Si-CNFs and T^2 peaks of the propyl trimethoxysilane treated

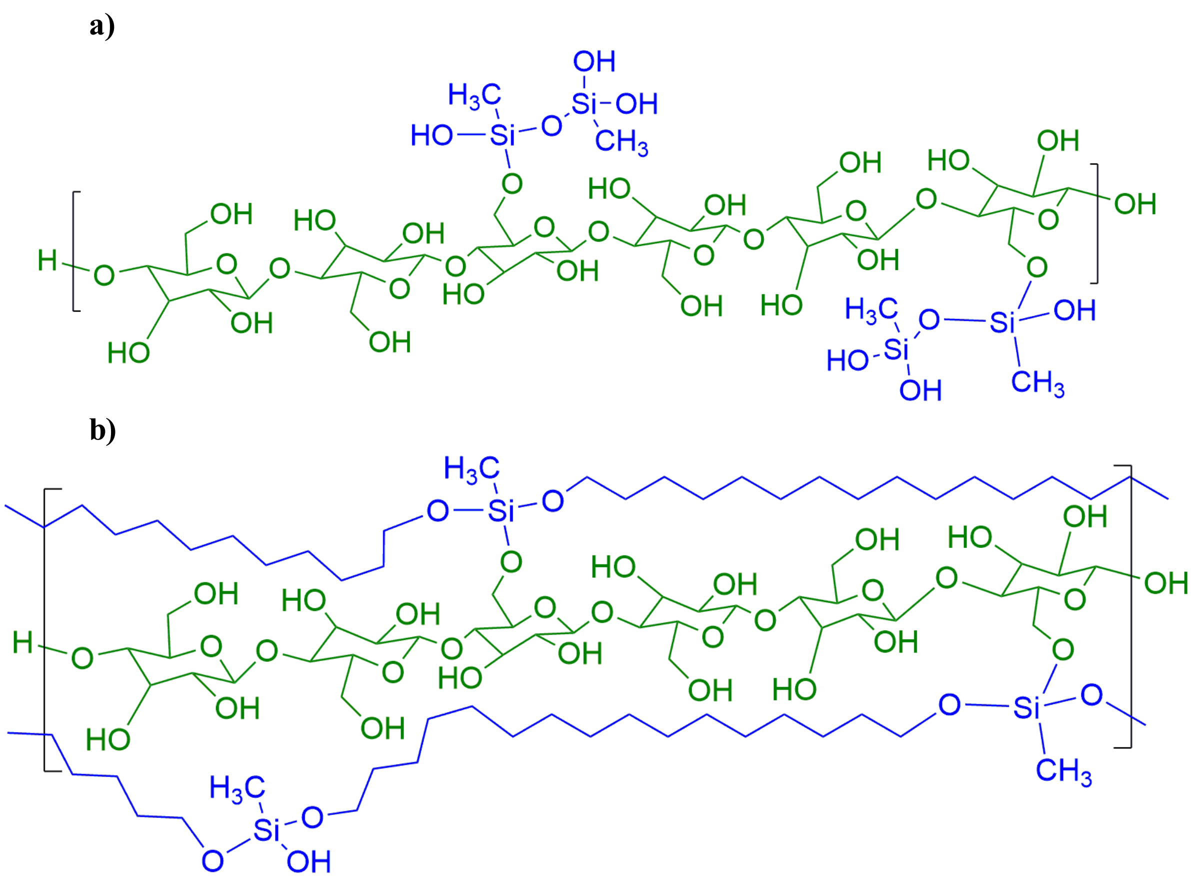

Figure 9. Schematics of approximate structures for 0.1Me-CNF (a) and 10Me-CNF (b). For both 0.1Me-CNF and 10Me-CNF, the siloxane coatings (blue) are attached to the CNFs (green) through a small number of covalent bonds. At a low degree of silanization (0.1Me-CNF), a small portion of the CNFs is covered by siloxane. As the degree of silanization increases, the CNFs are essentially coated with siloxane (10Me-CNF). The schematics display a single CNF coated with siloxane to more easily illustrate the silanization, when in reality multiple fibrils were closely associated regardless of the amount of siloxane coating adhered to them. Additionally, in (b), the blue chain around the fibril should be assumed to be repeat $SiO_2(OH)(CH_3)$ siloxane units. Shorthand was used to facilitate interpretation of the schematic.

Si-CNFs were broadened relative to those of the corresponding self-condensation products (Table S5). Any covalent attachment between the siloxane coating and nanocellulose was sparse, however, as evidenced by the relatively small T^1 peaks in ^{29}Si-spectra, the concomitant lack of significant changes in the crystalline and amorphous regions in ^{13}C-spectra, and the subtle differences in the cellulose region between the spectra of self-condensed, silane-treated, and untreated (^{13}C only) materials. This assertion is consistent with the results of previous NMR investigations of silanized nanocellulose.[82-83] The proposed approximate nature of the silanized CNFs is illustrated in Figure 9, where representative MTMS-modified Si-CNFs with relatively low and high coverages of siloxane coating are shown as an example. XPS indicated that as the degree of silanization increased, the fraction of coated CNFs also increased. Thus, in 0.1Me-CNF, only a small portion of the fibrils have a siloxane coating (Figure 9a), while the majority of the sample surface is still unmodified CNF. Increased silanization as in 10Me-CNF leads to most, if not all fibrils being coated in siloxane, with minimal nanocellulose exposed (Figure 9b). The thickness of this coating in 10Me-CNF was calculated to be ~0.4 nm as determined by the decrease in the cellulosic C–O peak intensity at 286.6 eV between the unmodified CNFs and 10Me-CNF (see Figure 3a).[84]

Dispersion Properties of Si-CNFs

The siloxane coated structure of the Si-CNFs described in Figure 9 served as the basis to explain their dispersion properties. The instability of unmodified CNF in chloroform is a consequence of the unfavorable intermolecular forces that exist between the hydrophilic surface of the nanocellulose and the hydrophobic solvent compared to the favorable interactions between adjacent nanofibrils. Silanization with MTMS improved the hydrophobicity of CNF, as 0.1Me-, 1Me-, 5Me-, and 10Me-CNF all displayed higher stability in chloroform compared to unmodified CNF. We ascribe this increase in CNF stability to the formation of an extensive and adherent hydrophobic siloxane coating, which led to improved hydrophobic intermolecular interactions between the Si-CNFs and chloroform. The net result was a stable dispersion which manifested as a suspended gel-like layer in solution for 5Me-CNF and 10Me-CNF. In 0.1Me-CNF and 1Me-CNF, the degree of silanization was lessened, which resulted in a smaller fraction of the sample suspended in chloroform due to lacking a sufficient siloxane coating.

Differences in the relative stability of CNFs coated with each type of siloxane can also be rationalized based on differences in the relative hydrophobicity of the coating. The high degree of stability for MTMS- and PTMS-modified CNFs can be attributed to the hydrophobic alkyl chains in the silane R_1-groups. In contrast, the polar terminal amino group in APTMS rendered this siloxane coating more hydrophilic relative to MTMS and PTMS modifications, and therefore less effective at improving the stability of CNF. We note that APTMS-modified CNFs still disperse more effectively than unmodified CNF, most likely due to the hydrophobic nature of both the Si–O linkages and the alkyl R_1 side chain.

The prolonged suspension of Si-CNFs in chloroform—a common solvent used in solvent casting—translated into improved CNF dispersion in polymer nanocomposites synthesized through solution blending with polyhydroxyalkanoates (PHA). The evaporation of solvent during the synthesis of these nanocomposites usually occurred over 1-2 h, which underlined the importance of CNF stability in the casting solution over this time span. In the case of unmodified CNF in the mass recovery tests, only 40% of the initial concentration remained in suspension over the first 2 h of settling in chloroform. Consequently, unmodified CNFs dispersed poorly in PHA as evidenced by the formation of aggregated patches of nanocellulose identified visually and with optical and electron microscopies (Figure 6).

The improved stability of silane-modified CNFs in chloroform translated into improved Si-CNF dispersion in CNF/PHA nanocomposites. This improvement can be understood when related to the mass recovery analyses of 5Me-CNF in chloroform, which retained 80% of its initial concentration in suspension after the first 2 h, and roughly maintained this concentration for the remainder of the 100 h. The relative uniformity of Si-CNF in PHA compared to unmodified CNF can reasonably be expected to lead to greater improvements in the material properties of PHA as compared to unmodified CNF, as demonstrated by previous studies.[10, 37, 52-55] As shown by these studies, uniform dispersion of nanofiller in polymer nanocomposites is a necessary condition to realize a sufficiently reinforced material. The presented data shows the direct relation between improved stability in solvent casting media and improved dispersion in polymer nanocomposites offered by CNF silanization, marking the materials described in this paper as representative of commercially utilized Si-CNFs.

Mineralization of Si-CNFs

We assessed the impact of silanization on the anaerobic mineralization of nanocellulose using biomethane potential tests to quantify the volume of biogas evolved.[56, 59] Efficient anaerobic mineralization involves a sequence of biodegradation steps which are initiated by the adsorption of a bacterial cell or multiprotein complex of enzymes onto the substrate. Complete conversion of cellulose to biogas requires exposure to a mixed culture of bacteria, as different bacterial species are required for each distinct step of mineralization in the absence of oxygen.[23] To meet this requirement, CNFs were exposed to anaerobic mixed cultures of microorganisms obtained from the digested sludge of a wastewater treatment plant. Here, it is important to make the distinction between whether a sample undergoes complete biodegradation, or mineralization. Complete biodegradation can be thought of as the total loss of sample mass due to bacterial metabolism. This includes both the portion of sample which is mineralized into biogas, and the portion that is broken down into nonvolatile small molecular species or water. In the case of anaerobic biodegradation by a mixed culture, cellulose is expected to be efficiently mineralized into biogas (i.e., carbon dioxide and methane) almost entirely, with little to no nonvolatile species being evolved.[23] Unmodified CNF rapidly mineralizes, as expected,[85] because bacteria and relevant enzymes are able to quickly access and adsorb onto the surface of the CNFs. After the bacteria adsorb, primary biodegradation begins with the enzymatic cleavage of glycosidic linkages in the biopolymer chain to yield cellobiose and glucose molecules.[23, 86] In anoxic environments, the complete biodegradation of these intermediate species can be concluded through mineralization into biogas consisting of methane and carbon dioxide. Due to the near complete conversion of cellulose into biogas, tracking the mineralization of nanocellulose samples is a reliable measure of their overall biodegradability.

Our data indicated that Si-CNF mineralization was either inhibited or completely ceased compared to unmodified CNF, depending on the degree of silanization as seen in Figure 7. These marked and systematic decreases in the rate and extent of CNF mineralization were ascribed to changes in the CNF surface chemistry due to the siloxane coatings. Figure 7 shows that as CNFs were increasingly coated with siloxane, the nanocellulose became systematically less susceptible to mineralization. We concluded that this effect occurred at high siloxane loadings because all fibril surfaces were completely and uniformly coated with a siloxane layer (ca. 0.4 nm as determined by XPS), rendering the nanocellulose (i.e., glycosidic linkages) inaccessible to bacteria and enzymes, and therefore non-biodegradable during the 4-month evaluation period. This interpretation also explains the intermediate degree of mineralization of CNFs modified with 1 and 5 wt% silane; in these instances, an incomplete coating of the fibrils with siloxane was achieved, which allowed for mineralization to occur, albeit to a lesser extent than in unmodified CNFs.

In addition to the relationship between the degree of silanization and CNF mineralization, samples treated with 5 wt% silane exhibited noticeable delays in the onset of degradation. In each 5 wt% silanized CNF, a steep rise in biogas production occurred around day 10 or later, while in less silanized samples, this rise took place at day 3. We concluded that for the 5Me-, 5A-, and 5P-CNF samples, the delay in biogas production was a result of hindered bacterial access to the nanocellulose due to a critical level of siloxane coating. This extent of coating disallowed primary biodegradation from proceeding (i.e., cleavage of glycosidic linkages) until the uncoated regions were accessed. Once this foothold was established, further mineralization of the primary biodegradation byproducts was enabled, resulting in the typical sinusoidal biogas production displayed in Figure 7.

Our data also suggest that the extent of CNF mineralization decreased as more highly hydrophobic silanization reagents were used (Figure 8). This trend could possibly be explained through the formation of a superhydrophobic coating on the CNF via the polymerization of PTMS[87] and MTMS.[88] In contrast, APTMS alone cannot impart superhydrophobicity due to its polar amino group, and would require the grafting of other reagents to achieve this effect.[89] As superhydrophobic surfaces have been shown to exhibit decreased bacterial attachment relative to moderately hydrophobic surfaces,[90] we would indeed expect PTMS- and MTMS-coated CNFs to be less prone to mineralization than the moderately hydrophobic APTMS-coated CNFs.

These findings also provide a means to help better understand previous studies involving the biodegradation of composites containing silanized cellulosic materials. Although the number of such studies is limited, composites that contain silanized cellulosic materials are generally less biodegradable than those which contain the unmodified cellulosic materials.[91-94] However, the magnitude of inhibition varies. For example, Way *et al.* indicated that PLA composites filled with silanized wood fibers displayed comparable or slightly improved biodegradation compared to PLA impregnated with the unmodified fibers.[91] Conversely, Jandas *et al.* observed that PLA loaded with silanized banana fibers biodegraded to a lesser degree than PLA loaded with unmodified banana fibers.[92] Results from our studies suggest that these differences are at least in part a reflection of differences in the extent of silanization, which is not typically measured. Furthermore, these previous studies do not address the fate of the modified nanocellulose filler after polymer degradation, which our data suggests will most likely persist as a result of the silanization.

In summary, our data demonstrate that while silane modification indeed improves the dispersion of nanocellulose in solvent cast polymer composites, it negatively impacts CNF mineralization. The magnitude of both effects scaled with the extent and hydrophobicity of siloxane coating. When completely covered in a siloxane coating, nanocellulose remained stable in solvent casting media over the course of 100 h, which led to an improved dispersion of these Si-CNFs in hydrophobic polymer composites. This is important, as uniform nanofiller dispersion is crucial for efficient transfer of CNF properties to the nanocomposite.[31-33]. While this improved material reinforcement is desired commercially, nanocellulose heavily modified with siloxane coatings is shown to be much more resistant to mineralization relative to the native CNF, thus increasing its environmental persistence. Therefore, in cases where materials featuring an environmentally transient nanofiller is desirable, such as in biomedical materials or products with transient use phases (e.g., packaging materials), nanocellulose extensively modified with silanes should be avoided. Conversely, in applications where non-biodegradable nanofillers are desired (e.g., in pipes or building materials), silane-modified nanocellulose could be used as an inexpensive, low weight nanofiller compared to other carbon-based options (i.e., CNTs, carbon fibers).

To avoid the issue of balancing the dispersion and biodegradability of nanocellulose, one potential solution is to covalently functionalize CNFs with small hydrophobic molecular species (e.g., esters).[38, 95] These molecular functionalization strategies could improve dispersion of nanocellulose in hydrophobic media without impacting its biodegradability by avoiding the formation of an inhibitory coating.

Conclusions

Cellulose nanofibrils were modified with three alkoxysilane reagents (MTMS, PTMS, APTMS) to determine the effect of hydrophobic silane modification on the dispersion and mineralization properties of nanocellulose. Silanization of CNFs resulted in the formation of a siloxane coating on the fibrils, the extent of which could be controlled based on the ratio of silane added to CNFs. Silanization did not change the cellulosic structure, crystallinity, or bonding in the CNFs, but improved CNF stability in chloroform by coating the hydrophilic nanocellulose surface with a hydrophobic siloxane layer. Improved stability of silanized CNFs in chloroform translated into improved dispersion of Si-CNFs in a hydrophobic polymer nanocomposite relative to unmodified CNFs, which instead aggregated extensively. Conversely, the extent to which silanized CNFs were mineralized decreased compared to unmodified CNFs, an effect attributable to the blocking of enzymatic cleavage sites by the siloxane coating. Indeed, no mineralization was observed for fully coated CNFs, indicating that such fillers and the materials featuring them would likely persist in the environment for increased periods of time when they are discarded at the end of consumer life. This study demonstrates the ability to control the biodegradability of nanocellulose as a function of its degree of silanization, while also highlighting the inverse relationship between dispersion and biodegradability and thus the need to determine the effect of surface modification strategies on environmentally relevant properties of CNFs in addition to their dispersion properties before commercial use and widespread implementation.

Acknowledgements

This work was supported by National Science Foundation under the Center for Sustainable Nanotechnology, CHE-1503408. The CSN is part of the Centers for Chemical Innovation Program. J.A.P. acknowledges support from the William A. Rothermel Bascom Professorship. Johns Hopkins would like to thank Chris Krout from the Back River Waste Water Treatment Plant (Baltimore, MD). This study made use of the National Magnetic Resonance Facility at Madison, which is supported by NIH grants P41 GM103399 (NIGMS) and P41GM66326 (NIGMS). Additional equipment was purchased with funds from the University of Wisconsin, the NIH (RR02781, RR08438), the NSF (DMB-8415048, OIA-9977486, BIR-9214394), and the USDA.

References

1. Moon, R. J.; Martini, A.; Nairn, J.; Simonsen, J.; Youngblood, J. Cellulose Nanomaterials Review: Structure, Properties and Nanocomposites. *Chem. Soc. Rev.* **2011,** *40* (7), 3941-3994.
2. Sacui, I. A.; Nieuwendaal, R. C.; Burnett, D. J.; Stranick, S. J.; Jorfi, M.; Weder, C.; Foster, E. J.; Olsson, R. T.; Gilman, J. W. Comparison of the Properties of Cellulose Nanocrystals and Cellulose Nanofibrils Isolated from Bacteria, Tunicate, and Wood Processed Using Acid, Enzymatic, Mechanical, and Oxidative Methods. *ACS Appl. Mater. Interfaces* **2014,** *6* (9), 6127-6138.
3. Chattopadhyay, D. Synthesis, Characterization and Application of Nano Cellulose for Enhanced Performance of Textiles. *Journal of Textile Science & Engineering* **2016,** *6* (2).
4. He, M.; Cho, B.-U.; Won, J. M. Effect of Precipitated Calcium Carbonate—Cellulose Nanofibrils Composite Filler on Paper Properties. *Carbohydr. Polym.* **2016,** *136* (Supplement C), 820-825.
5. Wei, H.; Rodriguez, K.; Renneckar, S.; Vikesland, P. J. Environmental Science and Engineering Applications of Nanocellulose-Based Nanocomposites. *Environ. Sci.: Nano* **2014,** *1* (4), 302-316.
6. Azeredo, H. M. C.; Rosa, M. F.; Mattoso, L. H. C. Nanocellulose in Bio-Based Food Packaging Applications. *Ind. Crops. Prod.* **2017,** *97*, 664-671.
7. Lin, N.; Dufresne, A. Nanocellulose in Biomedicine: Current Status and Future Prospect. *Eur. Polym. J.* **2014,** *59*, 302-325.
8. Sun, X.; Wu, Q.; Lee, S.; Qing, Y.; Wu, Y. Cellulose Nanofibers as a Modifier for Rheology, Curing and Mechanical Performance of Oil Well Cement. *Sci. Rep.* **2016,** *6*, 31654.
9. Xu, X.; Liu, F.; Jiang, L.; Zhu, J. Y.; Haagenson, D.; Wiesenborn, D. P. Cellulose Nanocrystals vs. Cellulose Nanofibrils: A Comparative Study on their Microstructures and Effects as Polymer Reinforcing Agents. *ACS Appl. Mater. Interfaces* **2013,** *5* (8), 2999-3009.

10. Lu, J.; Askeland, P.; Drzal, L. T. Surface Modification of Microfibrillated Cellulose for Epoxy Composite Applications. *Polymer* **2008,** *49* (5), 1285-1296.
11. Dufresne, A. *Nanocellulose: From Nature to High Performance Tailored Materials*. Walter de Gruyter: Berlin, Germany, 2012.
12. Hamid, S. B. A.; Zain, S. K.; Das, R.; Centi, G. Synergic Effect of Tungstophosphoric Acid and Sonication for Rapid Synthesis of Crystalline Nanocellulose. *Carbohydr. Polym.* **2016,** *138*, 349-355.
13. Feng, Y.-H.; Cheng, T.-Y.; Yang, W.-G.; Ma, P.-T.; He, H.-Z.; Yin, X.-C.; Yu, X.-X. Characteristics and Environmentally Friendly Extraction of Cellulose Nanofibrils from Sugarcane Bagasse. *Ind. Crops. Prod.* **2018,** *111* (Supplement C), 285-291.
14. Yadav, C.; Saini, A.; Maji, P. K. Energy Efficient Facile Extraction Process of Cellulose Nanofibres and their Dimensional Characterization Using Light Scattering Techniques. *Carbohydr. Polym.* **2017,** *165* (Supplement C), 276-284.
15. Phanthong, P.; Karnjanakom, S.; Reubroycharoen, P.; Hao, X.; Abudula, A.; Guan, G. A Facile One-Step Way for Extraction of Nanocellulose with High Yield by Ball Milling with Ionic Liquid. *Cellulose* **2017,** *24* (5), 2083-2093.
16. Henriksson, M.; Henriksson, G.; Berglund, L. A.; Lindström, T. An Environmentally Friendly Method for Enzyme-Assisted Preparation of Microfibrillated Cellulose (MFC) Nanofibers. *Eur. Polym. J.* **2007,** *43* (8), 3434-3441.
17. Carpenter, A. W.; de Lannoy, C. F.; Wiesner, M. R. Cellulose Nanomaterials in Water Treatment Technologies. *Environ. Sci. Technol.* **2015,** *49* (9), 5277-5287.
18. Das, S. Life Cycle Assessment of Carbon Fiber-Reinforced Polymer Composites. *Int. J. Life. Cycle. Assess.* **2011,** *16* (3), 268-282.
19. Akhshik, M.; Panthapulakkal, S.; Tjong, J.; Sain, M. Life Cycle Assessment and Cost Analysis of Hybrid Fiber-Reinforced Engine Beauty Cover in Comparison with Glass Fiber-Reinforced Counterpart. *EIA Review* **2017,** *65* (Supplement C), 111-117.
20. Sarma, S. J.; Bhattacharya, I.; Brar, S. K.; Tyagi, R. D.; Surampalli, R. y. Carbon Nanotube—Bioaccumulation and Recent Advances in Environmental Monitoring. *Crit. Rev. Environ. Sci. Technol.* **2015,** *45* (9), 905-938.
21. Petersen, E. J.; Akkanen, J.; Kukkonen, J. V. K.; Weber, W. J. Biological Uptake and Depuration of Carbon Nanotubes by Daphnia Magna. *Environ. Sci. Technol.* **2009,** *43* (8), 2969-2975.
22. Abbate, C.; Giorgianni, C.; Brecciaroli, R.; Giacobbe, G.; Costa, C.; Cavallari, V.; Albiero, F.; Catania, S.; Tringali, M. A.; Martino, L. B.; Abbate, S. Changes Induced by Exposure of the Human Lung to Glass Fiber–Reinforced Plastic. *Environ. Health Perspect.* **2006,** *114* (11), 1725-1729.
23. Leschine, S. B. Cellulose Degradation in Anaerobic Environments. *Annu. Rev. Microbiol.* **1995,** *49* (1), 399-426.
24. Arvidsson, R.; Nguyen, D.; Svanström, M. Life Cycle Assessment of Cellulose Nanofibrils Production by Mechanical Treatment and Two Different Pretreatment Processes. *Environ. Sci. Technol.* **2015,** *49* (11), 6881-6890.
25. Li, Q.; McGinnis, S.; Sydnor, C.; Wong, A.; Renneckar, S. Nanocellulose Life Cycle Assessment. *ACS Sustainable Chem. Eng.* **2013,** *1* (8), 919-928.
26. Oksman, K.; Etang, J. A.; Mathew, A. P.; Jonoobi, M. Cellulose Nanowhiskers Separated from a Bio-Residue from Wood Bioethanol Production. *Biomass & Bioenergy* **2011,** *35* (1), 146-152.
27. Roman, M.; Winter, W. T. Effect of Sulfate Groups from Sulfuric Acid Hydrolysis on the Thermal Degradation Behavior of Bacterial Cellulose. *Biomacromolecules* **2004,** *5* (5), 1671-1677.
28. Liu, C.-X.; Choi, J.-W. Improved Dispersion of Carbon Nanotubes in Polymers at High Concentrations. *Nanomaterials* **2012,** *2* (4), 329-347.
29. Bhattacharya, M. Polymer Nanocomposites—A Comparison Between Carbon Nanotubes, Graphene, and Clay as Nanofillers. *Materials* **2016,** *9* (4), 262.
30. Kaler, V.; Pandel, U.; Duchaniya, R. K. Development of TiO_2/PVA Nanocomposites for Application in Solar Cells. *Materials Today: Proceedings* **2018,** *5* (2, Part 1), 6279-6287.

31. Uddin, M. F.; Sun, C.-T. Effect of Nanoparticle Dispersion on Polymer Matrix and their Fiber Nanocomposites. In *Major Accomplishments in Composite Materials and Sandwich Structures*, Daniel, I. M.; Gdoutos, E. E.; Rajapakse, Y. D. S., Eds. Springer Netherlands: Dordrecht, 2010; pp 693-715.
32. Liu, T.; Phang, I. Y.; Shen, L.; Chow, S. Y.; Zhang, W.-D. Morphology and Mechanical Properties of Multiwalled Carbon Nanotubes Reinforced Nylon-6 Composites. *Macromolecules* **2004,** *37* (19), 7214-7222.
33. Müller, K.; Bugnicourt, E.; Latorre, M.; Jorda, M.; Echegoyen Sanz, Y.; Lagaron, J. M.; Miesbauer, O.; Bianchin, A.; Hankin, S.; Bölz, U.; Pérez, G.; Jesdinszki, M.; Lindner, M.; Scheuerer, Z.; Castelló, S.; Schmid, M. Review on the Processing and Properties of Polymer Nanocomposites and Nanocoatings and their Applications in the Packaging, Automotive and Solar Energy Fields. *Nanomaterials* **2017,** *7* (4), 74.
34. Guzmán de Villoria, R.; Miravete, A. Mechanical Model to Evaluate the Effect of the Dispersion in Nanocomposites. *Acta Materialia* **2007,** *55* (9), 3025-3031.
35. Tessema, A.; Zhao, D.; Moll, J.; Xu, S.; Yang, R.; Li, C.; Kumar, S. K.; Kidane, A. Effect of Filler Loading, Geometry, Dispersion and Temperature on Thermal Conductivity of Polymer Nanocomposites. *Polymer Testing* **2017,** *57*, 101-106.
36. Ferreiro, V.; Schmidt, G.; Han, C.; Karim, A. Dispersion and Nucleating Effects of Clay Fillers in Nanocomposite Polymer Films. In *Polymer Nanocomposites*, American Chemical Society: 2001; Vol. 804, pp 177-191.
37. Nakatani, H.; Iwakura, K.; Miyazaki, K.; Okazaki, N.; Terano, M. Effect of Chemical Structure of Silane Coupling Agent on Interface Adhesion Properties of Syndiotactic Polypropylene/Cellulose Composite. *J. Appl. Polym. Sci.* **2011,** *119* (3), 1732-1741.
38. Espino-Pérez, E.; Domenek, S.; Belgacem, N.; Sillard, C.; Bras, J. Green Process for Chemical Functionalization of Nanocellulose with Carboxylic Acids. *Biomacromolecules* **2014,** *15* (12), 4551-4560.
39. Song, Z.; Xiao, H.; Zhao, Y. Hydrophobic-Modified Nano-Cellulose Fiber/PLA Biodegradable Composites for Lowering Water Vapor Transmission Rate (WVTR) of Paper. *Carbohydr. Polym.* **2014,** *111*, 442-448.
40. Guo, J.; Fang, W.; Welle, A.; Feng, W.; Filpponen, I.; Rojas, O. J.; Levkin, P. A. Superhydrophobic and Slippery Lubricant-Infused Flexible Transparent Nanocellulose Films by Photoinduced Thiol–ene Functionalization. *ACS Appl. Mater. Interfaces* **2016,** *8* (49), 34115-34122.
41. Missoum, K.; Belgacem, M. N.; Bras, J. Nanofibrillated Cellulose Surface Modification: A Review. *Materials* **2013,** *6* (5), 1745-1766.
42. Kalia, S.; Dufresne, A.; Cherian, B. M.; Kaith, B. S.; Averous, L.; Njuguna, J.; Nassiopoulos, E. Cellulose-Based Bio- and Nanocomposites: A Review. *Int. J. Polym. Sci.* **2011,** *2011*.
43. Sair, S.; Oushabi, A.; Kammouni, A.; Tanane, O.; Abboud, Y.; Oudrhiri Hassani, F.; Laachachi, A.; El Bouari, A. Effect of Surface Modification on Morphological, Mechanical and Thermal Conductivity of Hemp Fiber: Characterization of the Interface of Hemp –Polyurethane Composite. *Case Stud. in Therm. Eng.* **2017,** *10*, 550-559.
44. Singh, G. Biodegradation of Nanocellulose and Microbial Community Response: Effect of Surface Modification and Morphology. Ph.D. Thesis, Virginia Polytechnic Institute and State University, Blacksburg, VA, 2015.
45. Cowie, J.; Bilek, E. M.; Wegner, T. H.; Shatkin, J. A. Market Projections of Cellulose Nanomaterial-Enabled Products--Part 2: Volume Estimates. *TAPPI J.* **2014,** *13* (6), 57-69.
46. Shatkin, J. A.; Wegner, T. H.; Bilek, E. M.; Cowie, J. Market Projections of Cellulose Nanomaterial-Enabled Products- Part 1: Applications. *TAPPI J.* **2014,** *13* (5), 9-16.
47. Barari, B.; Ellingham, T. K.; Ghamhia, I. I.; Pillai, K. M.; El-Hajjar, R.; Turng, L.-S.; Sabo, R. Mechanical Characterization of Scalable Cellulose Nano-fiber Based Composites Made Using Liquid Composite Molding Process. *Composites Part B: Engineering* **2016,** *84*, 277-284.

48. Raquez, J. M.; Murena, Y.; Goffin, A. L.; Habibi, Y.; Ruelle, B.; DeBuyl, F.; Dubois, P. Surface-Modification of Cellulose Nanowhiskers and their Use as Nanoreinforcers into Polylactide: A Sustainably-Integrated Approach. *Compos. Sci. Technol.* **2012,** *72* (5), 544-549.
49. Xu, S. H.; Gu, J.; Luo, Y. F.; Jia, D. M. Effects of Partial Replacement of Silica with Surface Modified Nanocrystalline Cellulose on Properties of Natural Rubber Nanocomposites. *Express Polym. Lett.* **2012,** *6*, 14-25.
50. Montes, S.; Azcune, I.; Cabañero, G.; Grande, H.-J.; Odriozola, I.; Labidi, J. Functionalization of Cellulose Nanocrystals in Choline Lactate Ionic Liquid. *Materials* **2016,** *9* (7), 499.
51. Xiaofei, D.; Xinyu, C.; Linnan, K.; Yongmei, M.; Jingjing, A.; Fosong, W. Combination of Cellulose Nanofibers and Chain-End-Functionalized Polyethylene and their Applications in Nanocomposites. *J. Appl. Polym. Sci.* **2017,** *134* (42), 45387.
52. Robles, E.; Urruzola, I.; Labidi, J.; Serrano, L. Surface-Modified Nano-Cellulose as Reinforcement in Poly(Lactic Acid) to Conform New Composites. *Ind. Crops. Prod.* **2015,** *71*, 44-53.
53. Kargarzadeh, H.; M. Sheltami, R.; Ahmad, I.; Abdullah, I.; Dufresne, A. Cellulose Nanocrystal: A Promising Toughening Agent for Unsaturated Polyester Nanocomposite. *Polymer* **2015,** *56*, 346-357.
54. Pickering, K. L.; Abdalla, A.; Ji, C.; McDonald, A. G.; Franich, R. A. The Effect of Silane Coupling Agents on Radiata Pine Fibre for Use in Thermoplastic Matrix Composites. *Compos. Part A Appl. Sci. Manuf.* **2003,** *34* (10), 915-926.
55. Colom, X.; Carrasco, F.; Pagès, P.; Cañavate, J. Effects of Different Treatments on the Interface of HDPE/Lignocellulosic Fiber Composites. *Compos. Sci. Technol.* **2003,** *63* (2), 161-169.
56. Owen, W. F.; Stuckey, D. C.; Healy, J. B.; Young, L. Y.; McCarty, P. L. Bioassay for monitoring biochemical methane potential and anaerobic toxicity. *Water Res.* **1979,** *13* (6), 485-492.
57. Xie, Y.; Hill, C. A. S.; Xiao, Z.; Militz, H.; Mai, C. Silane Coupling Agents Used for Natural Fiber/Polymer Composites: A Review. *Compos. Part A Appl. Sci. Manuf.* **2010,** *41* (7), 806-819.
58. Goodwin, D. G.; Boyer, I.; Devahif, T.; Gao, C.; Frank, B. P.; Lu, X.; Kuwama, L.; Gordon, T. B.; Wang, J.; Ranville, J. F.; Bouwer, E. J.; Fairbrother, D. H. Biodegradation of Carbon Nanotube/Polymer Nanocomposites Using a Monoculture. *Environ. Sci. Technol.* **2018,** *52* (1), 40-51.
59. Angelidaki, I.; Sanders, W. Assessment of the Anaerobic Biodegradability of Macropollutants. *Rev. Environ. Sci. Biotechnol.* **2004,** *3* (2), 117-129.
60. Chinga-Carrasco, G. Cellulose Fibres, Nanofibrils and Microfibrils: The Morphological Sequence of MFC Components from a Plant Physiology and Fibre Technology Point of View. *Nanoscale Res. Lett.* **2011,** *6* (1), 417-417.
61. Klemm, D.; Philipp, B.; Heinze, T.; Heinze, U.; Wagenknecht, W. Analytical Methods in Cellulose Chemistry: Section 3.3. In *Comprehensive Cellulose Chemistry*, Wiley-VCH Verlag GmbH & Co. KGaA: 2004; pp 181-195.
62. Ingale, S. V.; Wagh, P. B.; Tripathi, A. K.; Kamble, V. S.; Kumar, R.; Gupta, S. C. Physico-Chemical Properties of Silica Aerogels Prepared from TMOS/MTMS Mixtures. *J. Porous Mater.* **2011,** *18* (5), 567-572.
63. Tanaka, T. The Infrared Spectra of Methoxy-, Methylmethoxy- and Methoxy Endblocked Dimethyl-Polysiloxanes. *Bull. Chem. Soc. Jpn.* **1958,** *31* (6), 762-766.
64. Devouge, S.; Conti, J.; Goldsztein, A.; Gosselin, E.; Brans, A.; Voué, M.; De Coninck, J.; Homblé, F.; Goormaghtigh, E.; Marchand-Brynaert, J. Surface Functionalization of Germanium ATR Devices for Use in FTIR-Biosensors. *J. Colloid Interface Sci.* **2009,** *332* (2), 408-415.
65. Sánchez-Fernández, A.; Peña-Parás, L.; Vidaltamayo, R.; Cué-Sampedro, R.; Mendoza-Martínez, A.; Zomosa-Signoret, V.; Rivas-Estilla, A.; Riojas, P. Synthesization, Characterization, and In Vitro Evaluation of Cytotoxicity of Biomaterials Based on Halloysite Nanotubes. *Materials* **2014,** *7* (12), 7770.
66. Shimizu, I.; Okabayashi, H.; Taga, K.; Nishio, E.; O'Connor, C. J. Diffuse Reflectance Infrared Fourier Transform Spectral Study of the Thermal and Adsorbed-Water Effects of a 3-Aminopropyltriethoxysilane Layer Modified onto the Surface of Silica Gel. *Vib. Spectrosc.* **1997,** *14* (1), 113-123.

67. Saal, K.; Tätte, T.; Tulp, I.; Kink, I.; Kurg, A.; Mäeorg, U.; Rinken, A.; Lõhmus, A. Sol–Gel Films for DNA Microarray Applications. *Mater. Lett.* **2006,** *60* (15), 1833-1838.
68. Johansson, L.-S.; Tammelin, T.; Campbell, J. M.; Setala, H.; Osterberg, M. Experimental Evidence on Medium Driven Cellulose Surface Adaptation Demonstrated Using Nanofibrillated Cellulose. *Soft Matter* **2011,** *7* (22), 10917-10924.
69. Loof, D.; Hiller, M.; Oschkinat, H.; Koschek, K. Quantitative and Qualitative Analysis of Surface Modified Cellulose Utilizing TGA-MS. *Materials* **2016,** *9* (6), 415.
70. Glaser, R. H.; Wilkes, G. L. Structure Property Behavior of Polydimethylsiloxane and Poly(Tetramethylene Oxide) Modified TEOS Based Sol-Gel Materials. *Polymer Bulletin* **1988,** *19* (1), 51-57.
71. Hasegawa, I.; Sakka, S.; Sugahara, Y.; Kuroda, K.; Kato, C. Polymerization of Hydrolysis Products of Methyltriethoxysilane in Aqueous Solutions. *Journal of the Ceramic Society of Japan* **1990,** *98* (1139), 647-652.
72. Salon, M.-C. B.; Gerbaud, G.; Abdelmouleh, M.; Bruzzese, C.; Boufi, S.; Belgacem, M. N. Studies of Interactions Between Silane Coupling Agents and Cellulose Fibers with Liquid and Solid-State NMR. *Magn. Reson. Chem.* **2007,** *45* (6), 473-483.
73. Sindorf, D. W.; Maciel, G. E. Solid-state NMR Studies of the Reactions of Silica Surfaces with Polyfunctional Chloromethylsilanes and Ethoxymethylsilanes. *Journal of the American Chemical Society* **1983,** *105* (12), 3767-3776.
74. Alam, T. M.; Assink, R. A.; Loy, D. A. Hydrolysis and Esterification in Organically Modified Alkoxysilanes: A 29Si NMR Investigation of Methyltrimethoxysilane. *Chemistry of Materials* **1996,** *8* (9), 2366-2374.
75. Henrichs, M. P.; Nicely, V. A. An Experimental Determination of the Local Chain Conformation of Bisphenol A Polycarbonate. *Macromolecules* **1990,** *23* (12).
76. Osterholtz, F. D.; Pohl, E. R. Kinetics of the Hydrolysis and Condensation of Organofunctional Alkoxysilanes: A Review. *J. Adhes. Sci. Technol.* **1992,** *6* (1), 127-149.
77. Blum, F. D.; Meesiri, W.; Kang, H.-J.; Gambogi, J. E. Hydrolysis, Adsorption, and Dynamics of Silane Coupling Agents on Silica Surfaces. *J. Adhes. Sci. Technol.* **1991,** *5* (6), 479-496.
78. de Oliveira Taipina, M.; Ferrarezi, M. M. F.; Yoshida, I. V. P.; Gonçalves, M. d. C. Surface Modification of Cotton Nanocrystals with a Silane Agent. *Cellulose* **2013,** *20* (1), 217-226.
79. Pinheiro, I. F.; Ferreira, F. V.; Souza, D. H. S.; Gouveia, R. F.; Lona, L. M. F.; Morales, A. R.; Mei, L. H. I. Mechanical, Rheological and Degradation Properties of PBAT Nanocomposites Reinforced by Functionalized Cellulose Nanocrystals. *Eur. Polym. J.* **2017,** *97* (Supplement C), 356-365.
80. Kint, D.; Muñoz-Guerra, S. A Review on the Potential Biodegradability of Poly(Ethylene Terephthalate). *Polym. Int.* **1999,** *48* (5), 346-352.
81. J., J. M.; L., H. K. The Effect of Crystalline Morphology on the Degradation of Polycaprolactone in a Solution of Phosphate Buffer and Lipase. *Polym. Advan. Technol.* **2008,** *19* (12), 1901-1906.
82. Abdelmouleh, M.; Boufi, S.; ben Salah, A.; Belgacem, M. N.; Gandini, A. Interaction of Silane Coupling Agents with Cellulose. *Langmuir* **2002,** *18* (8), 3203-3208.
83. Zhou, F.; Cheng, G.; Jiang, B. Effect of Silane Treatment on Microstructure of Sisal Fibers. *Appl. Surf. Sci.* **2014,** *292* (Supplement C), 806-812.
84. Jablonski, A.; Zemek, J. Overlayer Thickness Determination by XPS Using the Multiline Approach. *Surface and Interface Analysis* **2009,** *41* (3), 193-204.
85. Singh, G.; Chandoha-Lee, C.; Zhang, W.; Renneckar, S.; Vikesland, P. J.; Pruden, A. Biodegradation of Nanocrystalline Cellulose by Two Environmentally-Relevant Consortia. *Water Res.* **2016,** *104*, 137-146.
86. Lynd, L. R.; Weimer, P. J.; van Zyl, W. H.; Pretorius, I. S. Microbial Cellulose Utilization: Fundamentals and Biotechnology. *Microbiol. Mol. Biol. Rev.* **2002,** *66* (3), 506-577.
87. Ramanathan, R.; Weibel, D. E. Novel Liquid–Solid Adhesion Superhydrophobic Surface Fabricated Using Titanium Dioxide and Trimethoxypropyl Silane. *Appl. Surf. Sci.* **2012,** *258* (20), 7950-7955.

88. Karapanagiotis, I.; Pavlou, A.; Manoudis, P. N.; Aifantis, K. E. Water Repellent ORMOSIL Films for the Protection of Stone and Other Materials. *Mater. Lett.* **2014,** *131* (Supplement C), 276-279.
89. Li, L.; Li, B.; Dong, J.; Zhang, J. Roles of Silanes and Silicones in Forming Superhydrophobic and Superoleophobic Materials. *J. Mater. Chem. A* **2016,** *4* (36), 13677-13725.
90. Yuan, Y.; Hays, M. P.; Hardwidge, P. R.; Kim, J. Surface Characteristics Influencing Bacterial Adhesion to Polymeric Substrates. *RSC Adv.* **2017,** *7* (23), 14254-14261.
91. Way, C.; Dean, K.; Wu, D. Y.; Palombo, E. Biodegradation of Sequentially Surface Treated Lignocellulose Reinforced Polylactic Acid Composites: Carbon Dioxide Evolution and Morphology. *Polym. Degrad. Stab* **2012,** *97* (3), 430-438.
92. P.J., J.; S., M.; S.K., N.; H., S. Effect of Surface Treatments of Banana Fiber on Mechanical, Thermal, and Biodegradability Properties of PLA/Banana Fiber Biocomposites. *Polym. Compos.* **2011,** *32* (11), 1689-1700.
93. Calabia, B.; Ninomiya, F.; Yagi, H.; Oishi, A.; Taguchi, K.; Kunioka, M.; Funabashi, M. Biodegradable Poly(Butylene Succinate) Composites Reinforced by Cotton Fiber with Silane Coupling Agent. *Polymers* **2013,** *5* (1), 128.
94. Kittikorn, T.; Kongsuwan, S.; Malakul, R. Investigation of the Durability of Sisal Fiber/PLA Biocomposite Through Evaluation of Biodegradability by Means of Microbial Growth. *Journal of Metals, Materials and Minerals* **2017,** *27* (2), 23-34.

95. Eyley, S.; Thielemans, W. Surface Modification of Cellulose Nanocrystals. *Nanoscale* **2014,** *6*, 7764-7779.

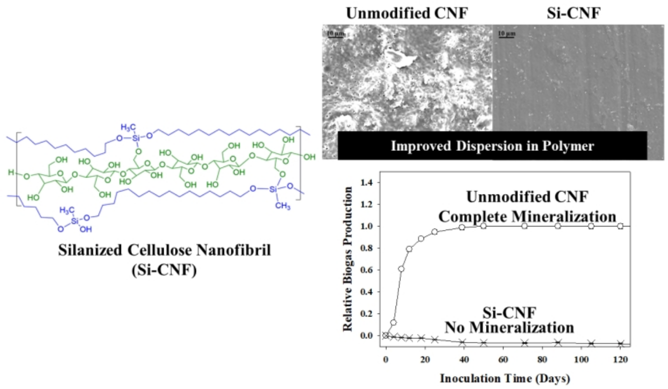

Silanization of cellulose nanofibrils improves the dispersion of the nanofibrils in polymer matrices but reduces the inherent biodegradability of the nanocellulose.

254x142mm (192 x 192 DPI)